Algal Research

Integrated experimental and photo-mechanistic modelling of biomass and optical density production of fast versus slow growing model cyanobacteria

--Manuscript Draft--

Manuscript Number:	ALGAL-D-22-00838R1
Article Type:	Full Length Article
Section/Category:	Algal Biotechnology
Keywords:	Cyanobacterial biotechnology; Synechococcus sp. PCC 11901; Synechocystis sp. PCC 6803; Light attenuation; Biomass and OD dynamic modelling
Corresponding Author:	Bovinille Anye Cho The University of Manchester Manchester, UNITED KINGDOM
First Author:	Bovinille Anye Cho
Order of Authors:	Bovinille Anye Cho
	José Ángel Moreno-Cabezuelo
	Lauren A. Mills
	Ehecatl Antonio del Río Chanona
	David J. Lea-Smith
	Dongda Zhang
Abstract:	Biotechnological exploitation of fast-growing cyanobacterial species is hindered by unavailable mechanistic interpretations for the differing bioconversion rates when exploring strains with similar metabolic pathways and transport systems. This study investigated two strains: Synechococcus sp. PCC 11901, the fastest growing cyanobacterium identified to date, and Synechocystis sp. PCC 6803, under a range of operational light intensities from 300 - 900 µmol photons m-2 s-1, and presents three original contributions. Firstly, strain specific dynamic biomass and optical density (OD750nm) models were constructed incorporating sophisticated photo-mechanistic influences, previously unachieved in OD750nm. Secondly, bootstrapping parameter estimation with 3-fold cross validations was exploited to simultaneously identify the model parameters and confidence intervals, thus enabling probabilistic simulations and thorough validation against experimental data sets. Thirdly, presented mechanistic interpretations for the over two-fold faster growth of PCC 11901 versus PCC 6803 despite PCC 6803's high light utilisation efficiency. These findings will benefit upscaling of future cyanobacterial biotechnology applications and exploitation of Synechococcus sp. PCC 11901 for production of biomass and chemicals of industrial, nutritional and medical importance.
Suggested Reviewers:	Keju Jing Professor, Xiamen University jkj@xmu.edu.cn Expert in photo-production processes, bioprocess modelling, and photobioreactor design
	Pongsathon Dechatiwongse Professor, Walailak University pongsathorn.de@wu.ac.th Expert in cyanobacterial photo-production systems and bioprocess modelling. Research works were cited in this manuscript.
	Bojan Tamburic Lecturer, University of New South Wales b.tamburic@unsw.edu.au Expert in Algal photo-production modelling, design of experiments, photobioreactor design and biochemical engineering.
	Leonardo Rios Solis

	Senior Lecturer, Newcastle University Leo.Rios@ncl.ac.uk Expert in microbial cell factories, bioprocess modelling and biochemical reaction engineering.
Opposed Reviewers:	
Response to Reviewers:	

Centre for Process Integration
School of Engineering (Department of Chemical Engineering)
University of Manchester
Engineering Building A, Manchester, M13 9PL, UK
Tel: +44 (0) 744 848 5377
bovinille.anyecho@manchester.ac.uk

Mr. Bovinille Anye Cho, MEng, AMRSC

5th November 2022

The Editor-in-Chief, Algal Research

Dear Professor A. H. Buschmann,

Submission of original paper to your Journal

I am presently submitting to your Journal our original research paper entitled:

Integrated experimental and photo-mechanistic modelling of biomass and optical density production for the cyanobacterium Synechococcus sp. PCC 11901

I can confirm that this work is original and adheres to all the ethical and professional requirements set out in the Journal's and Elsevier's guidelines.

Paper summary and motivation:
In this work, sophisticated photomechanisms informed by experimental observations within 300 - 900 µmol photons m^{-2} s^{-1}, were incorporated in the dynamic biomass and optical density (OD_{750nm}) modelling of two cyanobacterial strains: *Synechococcus* sp. PCC 11901, the fastest growing cyanobacterium identified to date, and *Synechocystis* sp. PCC 6803 with similar metabolic pathways and transport systems. Whilst previously unachieved in OD_{750nm}, thus an original contribution, two other contributions were presented herein. These were (i) bootstrapping parameter estimation enabling probabilistic simulations, and thorough validation against experimental data sets, and (ii) mechanistic interpretations for the over two-fold faster growth of PCC 11901 versus PCC 6803 despite PCC 6803's high light utilisation efficiency.

We believe that our work is significant since using these models and findings will benefit upscaling of future cyanobacterial biotechnology applications, online bioprocess control, and exploitation of *Synechococcus* sp. PCC 11901 for production of biomass and chemicals of industrial, nutritional, and medical importance.

The list of authors including myself is: *Bovinille Anye Cho, José Ángel Moreno-Cabezuelo, Lauren A. Mills, Ehecatl Antonio del Río Chanona, David J. Lea-Smith, Dongda Zhang*

Sincerely yours,

Bovinille Anye Cho

Integrated experimental and photo-mechanistic modelling of biomass and optical density production of~~or~~ fast versus slow growing~~the~~ model cyanobacteria~~aum~~ ~~*Synechococcus* sp. PCC 11901~~

Commented [AB1]: This addresses the comment of reviewer 1 regarding title change.

Bovinille Anye Cho[1,*], José Ángel Moreno-Cabezuelo[2], Lauren A. Mills[2], Ehecatl Antonio del Río Chanona[3], David J. Lea-Smith[2], Dongda Zhang[1]

1. School of Engineering, Department of Chemical Engineering, University of Manchester, Engineering Building A, Oxford Road, Manchester, M13 9PL, UK.
2. School of Biological Sciences, University of East Anglia, Norwich Research Park, Norwich, NR4 7TJ, United Kingdom
3. Department of Chemical Engineering, Imperial College London, South Kensington Campus, London SW7 2AZ, UK.

*: Corresponding author, Bovinille Anye Cho: email: bovinille.anyecho@manchester.ac.uk, tel: 44 (0) 744 848 5377.

Abstract

Biotechnological exploitation of fast-growing cyanobacterial species is hindered by unavailable mechanistic interpretations for the differing bioconversion rates when exploring strains with similar metabolic pathways and transport systems. This study investigated two strains: *Synechococcus* sp. PCC 11901, the fastest growing cyanobacterium identified to date, and *Synechocystis* sp. PCC 6803, under a range of operational light intensities from 300 - 900 µmol photons m^{-2} s^{-1}, and presents three original contributions. Firstly, strain specific dynamic biomass and optical density (OD_{750nm}) models were constructed incorporating sophisticated photo-mechanistic influences, previously unachieved in OD_{750nm}. Secondly, bootstrapping parameter estimation with 3-fold cross validations was exploited to simultaneously identify the model parameters and confidence intervals, thus enabling probabilistic simulations and thorough validation against experimental data sets. Thirdly, presented mechanistic interpretations for the over two-fold faster growth of PCC 11901 versus PCC 6803 despite PCC 6803's high light utilisation efficiency. These findings will benefit upscaling of future cyanobacterial biotechnology applications and exploitation of *Synechococcus* sp. PCC 11901 for production of biomass and chemicals of industrial, nutritional and medical importance.

Keywords: Cyanobacterial biotechnology; *Synechococcus* sp. PCC 11901; *Synechocystis* sp. PCC 6803; Light attenuation; Biomass and OD dynamic modelling.

1. Introduction

Cyanobacteria are potential chassis for converting inorganic carbon into biomass and biomolecules for industrial (e.g., isoprene [1]), nutritional (e.g., glucose/fructose mixture [2]), medical (e.g., mycosporine and mycosporine-like amino acids [3]), and herbicidal (e.g., antimetabolite 7-deoxy-sedoheptulose [4]) applications. Utilising light, minimal nutrients and potentially low-cost waste streams like flue gases (e.g., 4-14 vol% CO_2 from power plants [5–7]), with facilities not requiring arable land, cyanobacterial production of biomolecules could be industrially attractive for carbon capture and the sustainable production of biorenewable compounds. However, to improve commerciality, overall cyanobacterial productivity (i.e., amount of product per time) and product titer (i.e., amount of product per volume) needs to be comparable to alternative industrially viable heterotrophic microorganisms like *Escherichia coli* and *Saccharomyces cerevisiae* with doubling times of 20 and 90 minutes, respectively [8].

For this reason, significant research efforts has been invested in isolating cyanobacterial species that grow faster than the most commonly studied and genetically tractable model organisms such as *Synechocystis* sp. PCC 6803 (PCC 6803) [8–10] and *Synechococcus elongatus* PCC 7942 (PCC 7942) [9,10] with doubling times of 6.6 and 4.1 hours, respectively [8]. *Synechococcus* sp. PCC 7002 (PCC 7002) [9–11] and more recently, *Synechococcus elongatus* UTEX 2973 (UTEX 2973) [9–12], and *Synechococcus* sp. PCC 11901 (PCC 11901) [8,10] with respective doubling times of 4.0 hours [8,9], 2.1 hours [9] and 2.0 hours [10], have been partially characterised. A comparison of these species showed that PCC 11901 demonstrated the fastest growth and highest biomass accumulation (up to 33 g DCW L^{-1} [10]), suggesting it is the most promising species for future biotechnology applications. Faster growth may be due to a range of factors but could be linked to lower photoinhibition, higher photosynthetic rates, and higher light utilisation efficiency in PCC 11901 than other model species [8]. Surprisingly, PCC 11901 and PCC 6803 were shown to have very similar metabolic pathways and transport

systems [8]. Despite these similarities, in-depth mechanistic analysis via estimated biokinetic model parameters, which could provide additional physical, chemical, biological and interacting explanations for the observed growth capabilities, have not been conducted. Previous studies either (i) directly compared the obtained final biomass concentrations and/or optical densities [10,13], and/or (ii) experimentally measured the oxygen evolution and photoinhibition rates [8], and/or (iii) curve fit for the maximum specific growth rate with the experimentally generated data of biomass concentrations and/or optical densities [10,12]. As a result, doubling times are grossly estimated without accounting for the impact of process equipment (e.g., photobioreactor path length), operation (e.g., light intensity and light attenuation), and growth dynamics (e.g., photolimitation, photosaturation and photoinhibition). This makes it challenging to compare PCC 11901 to industrially viable heterotrophic microorganisms with reported doubling times from scalable bioreactor layouts (i.e., lab to the industrial scale). For example, investigations of PCC 11901 have been so far limited to <100 mL PBRs [8] but directly compared to *Saccharomyces cerevisiae* investigations from a 1 L fermenter [14].

Combining experimental observations with dynamic mechanistic approaches has been exploited in previous studies. For example, Clark *et al*., [11] exploited dynamic models to compare light-limited cyanobacterial growth of PCC 7002 and UTEX 2973 in differing experimental systems by comparing their photosynthetic efficiencies. Unlike Clark *et al*., [11] whereby the growth dynamics were limited to the stationary growth phase, all other cyanobacterial growth phases (i.e., primary, secondary, and stationary) except the lag phase were comprehensively described mechanistically by Zhang *et al*., [15] and Del Rio-Chanona, *et al*., [16] for *Cyanothece* sp. ATCC 51142. Dechatiwongse *et al*., [17] implemented two dynamic models: a logistic model for optical density and an inverse logistic model for nutrient uptake, in describing the effects of light intensity and photoinhibition on *Cyanothece* sp. ATCC

51142. Although they investigated a wide range of light intensities (i.e., 23 to 320 µmol photons m^{-2} s^{-1}) in a 3L tubular Photobioreactor (PBR), the influence of light attenuation was not accounted for within their dynamic models.

Accounting for light attenuation is of utmost importance when analysing fast growing strains. In dense cultures, cells in the front-facing PBR section will harvest the majority of light, leading to higher levels of photoinhibition [18,19]. Cells in the interior will receive less light and may become photolimited, consequentially affecting the overall reported growth rate of the culture. These growth dynamics have been successfully modelled using the Beer-Lambert Law and Aiba model for light attenuation and photomechanisms (i.e., photolimitation, photosaturation and photoinhibition), respectively, in the literature [20–23]. However, these studies were mainly focused on the construction of dynamic biomass production models and the incorporation of light attenuation and photomechanisms into dynamic optical density models has not been performed.

To address these limitations we aim to embed the impact of light intensity, light attenuation, photolimitation, photosaturation and photoinhibition photomechanisms in assessment of growth via biomass accumulation and OD_{750nm} measurements, and scalability potential of two cyanobacterial species: PCC 11901 and PCC 6803. Specifically, we will: (i) analyse differences in biomass accumulation and growth via optical density measurements within a wide range of environmentally relevant light intensities from 300 to 900 µmol photons m^{-2} s^{-1}, (ii) construct dynamic predictive models for biomass production and optical density measurements, unifying the complicated influences of incident light intensity, light attenuation and photomechanisms to support the explanations of experimental results via comparison of the estimated biokinetic model parameters, and (iii) provide in-depth mechanistic discussion and identification of the optimal light intensities for cultivation and biotechnological scalabilities of the strains.

2. Materials and modelling methods

2.1 Bacterial species, media, and starter culture growth conditions

Two cyanobacterial species, PCC 11901 (a kind gift from Peter Nixon, Imperial College London) and PCC 6803 [24] were maintained on AD7 and BG11 agar plates, respectively, as previously described in [13] and [10]. Cells scraped off plates were used to seed starter cultures grown in their corresponding liquid medium of 50 mL in 100 mL conical flasks. Conical flasks were shaken at 120 rpm while being maintained at a temperature of 30 °C and under a light intensity of 40 µmol photons m^{-2} s^{-1} as provided by a warm white LED light in an Algaetron 230 growth chamber (Photon Systems Instruments, Czech Republic).

2.2 Photobioreactor setup and operation

Strains were cultured in 100 mL cultivation tubes in a MC-1000 multicultivator bioreactor equipped with a warm white LED light source having a radiating capacity up to 1000 µmol photons m^{-2} s^{-1} (Photon Systems Instruments, Czech Republic) (see Fig. 1). Each cultivation tube had an external and internal diameter of 30 mm and 27 mm, respectively. Cells were sparged with air/5% CO_2 to supplement the supply of inorganic carbon and mix the cells; this was maintained at a temperature of 38 °C. Optical density was quantified using a Jenway 6305 Genova UV/VIS (Genova, United Kingdom) spectrophotometer set at a wavelength of 750 nm. Initially, the PBR was illuminated at 150 µmol photons m^{-2} s^{-1} and 80 mL of its volume was inoculated with a starter culture of $\mathrm{OD}_{750\mathrm{nm}} = \sim 0.1$, before being incubated for 24 hours. Afterwards, the growing culture was diluted down to $\mathrm{OD}_{750\mathrm{nm}} = \sim 0.1$ and re-inoculated into the PBR for a stepped-up illuminating light intensity (Table 1) for another 24 hour period. Thereafter, the illuminating light intensity was further increased to the final target light intensity (Table 1) and the growing cultures were incubated overnight to adapt to the new PBR conditions. From this culture, samples were removed and diluted to $\mathrm{OD}_{750\mathrm{nm}} = 0.25$, before

starting the growth experiments at the various investigated light intensities (300, 450, 600, 750 and 900 µmol photons m^{-2} s^{-1}). Growth experiments lasted for 120 hours and 1 mL samples were removed for analysis from the PBR at 12 hours interval during this cultivation time.

2.3 Analytical methods

The state variables of interest herein were the (i) optical density measured at a wavelength of 750 nm ($\mathrm{OD}_{750\mathrm{nm}}$) and (ii) cell dry weight, X (g L^{-1}) (referred to as biomass concentration thereafter). Biomass concentration was determined from established standard curves between X and $\mathrm{OD}_{750\mathrm{nm}}$ as reported in Eq. (1) and (2) for PCC 11901 and PCC 6803 respectively. These standard curves were achieved by harvesting densely grown cultures from the PBR after 120 hours. Cells were centrifuged at 5,000 x g with a Centrifuge 5804 R (Eppendorf, Germany) and washed twice with sterile deionised water. The samples were diluted to 10%, 20%, 40%, 60%, 80% and 100%, recorded for $\mathrm{OD}_{750\mathrm{nm}}$ at each serial dilution, with 5 mL of the serial dilution aliquoted on a pre-weighed filter paper of 70 mm diameter (i.e., Whatman GF/B Glass Microfibre Filters, USA). Prior to this, the filter paper had been dried for 48 hours at 70°C in an oven (Binder BD-S 056, Germany) and then weighed with a microbalance (Kern ABT 220-SDNM, Germany). Cells on the dried filter paper were left at 24 hours at 70°C, then weighed in triplicate.

Commented [AB2]: This addresses the comment of reviewer 2 regarding typo.

$$X_{\mathrm{PCC\_11901}}(\mathrm{g\ L^{-1}}) = 0.222 \cdot OD_{750nm\_\mathrm{PCC\_11901}}\,, \quad \mathrm{R}^2 = 0.998 \tag{1}$$

$$X_{\mathrm{PCC\_6803}}(\mathrm{g\ L^{-1}}) = 0.2406 \cdot OD_{750nm\_\mathrm{PCC\_6803}}\,, \quad \mathrm{R}^2 = 0.996 \tag{2}$$

2.4 Mathematical model construction

The constructed dynamic models were used to simulate state variables under the sophisticated influences of (i) incident light intensity, (ii) light attenuation, and (iii) photomechanisms.

However, the differing magnitude of light related influences among the two investigated cyanobacterial strains implied their experimental data sets would first need to be subjected to statistical student *t*- test(s) to inform the incorporation of either all (i.e., (i), (ii) and (iii)) or a selective combination (e.g., (i) and (iii) only) of these light related influences.

2.4.1 Modelling of biomass concentrations

The two cyanobacterial species were expected to exhibit the four different growth phases (namely the (i) lag phase, (ii) primary growth phase (iii) secondary growth phase, and (iv) stationary phase), as reported in other studies [15–17]. Herein, the lag phase was not pronounced due to the starter cultures being adapted to the operational light intensity of the PBR by using the light stepping up strategy as reported in Table 1. Therefore, the dynamic model structure in Eq. (3) was constructed to capture the three remaining phases. This model structure permits the incorporation of the strain dependent biological knowledge influencing the trajectories of the state variables. For instance, the light related influences of differing magnitude among the cyanobacterial strains are linked to the growth associated terms (i.e., first term on right hand side of Eq. (3)). Meanwhile, the decay associated terms (i.e., second term on right hand side of Eq. (3)) are often controlled by endogenous cellular respiration activities, thus taking place under dark circumstances, and can be modelled as independent of light.

$$\frac{dX}{dt} = u\,(I) \cdot X - \mu_d \cdot X^2 \tag{3}$$

Where X is the biomass concentration (g L^{-1}), $u\,(I)$ represents the effects of the PBR's light intensities on the biomass growth (h^{-1}) and $\mu_d(I)$ denotes the specific cell decay rate (L g^{-1} h^{-1}).

2.4.2 Modelling of optical densities

Although often disputed as to whether there exist a linear or a non-linear correlation between the biomass concentration and optical density, the optical density profiles of *Synechococcus* and *Synechocystis* strains has been shown [8,10,17] to have sigmoidal shapes. This sigmoidal shape is typical of bioprocesses experiencing the three remainder phases as highlighted in Section 2.4.1. Thus, the model structure of the optical density and biomass concentration (i.e., Eq. (3)) were assumed to be similar. Hence, Eq. (4) was constructed to simulate the optical density profiles of the two cyanobacterial species.

$$\frac{d\ \mathrm{OD}_{750}}{dt} = u\ (I) \cdot\ \mathrm{OD}_{750} - \mu_d \cdot\ {\mathrm{OD}_{750}}^2 \tag{4}$$

Where OD_{750} is the optical density at a wavelength of 750 nm (dimensionless), $u\ (I)$ represents the effects of the PBR's light intensities on the optical density build up (h^{-1}) and μ_d denotes the specific rate of vanishing optical density (h^{-1}).

2.4.3 Modelling of light intensity, light attenuation, and photomechanisms

Generally, in the literature [15,19,20,23], the effect of light on growth rates are often characterised mechanistically by three distinguishable photomechanisms, namely (i) photolimitation, (ii) photosaturation and (iii) photoinhibition, via the Aiba model structure (Eq. (5)). The former, second and latter occur under low, optimal, and high light intensities, respectively. Under low light intensities, the growth rate increases linearly with increasing light intensity till saturation at the optimal light intensity. Beyond this, the growth rate decreases with further increase in the light intensity. Considering~~, and with~~ the wide range of investigated light intensities (300 – 900 µmol photons m^{-2} s^{-1}), it was necessary to implement a model that captures all three photomechanisms on the growth associated terms (i.e., first term on right hand side) of Eq. (3) and Eq. (4). However, student *t*- test(s) were first performed on the experimental data sets for statistical significance to confirm the validity of the light influences on the two cyanobacterial strains.

Commented [AB3]: This addresses the comments of reviewer 2 regarding additional details of the Aiba model.

$$u\ (I) = u_m \cdot \frac{I(z)}{I(z) + k_s + \frac{I(z)^2}{k_i}} \tag{5}$$

Where u_m is the maximum specific growth rate (h^{-1}), $I(z)$ denotes the light attenuation model (see Eqs. (6) and (7) below), k_s and k_i are the light saturation (µmol photons m^{-2} s^{-1}) and light inhibition (µmol photons m^{-2} s^{-1}) coefficients respectively.

2.4.3.1 Modelling PCC 11901 growth associated terms

From the student's *t*-test performed over the wide operational light intensity range (300 to 900 µmol photons m^{-2} s^{-1}), statistical significance ($P<0.05$ being statistically significant) of light intensity influences were observed in the data sets of PCC 11901 as further discussed in Section 3.1. Hence, Eq. (5) was employed to encompass all the above mentioned photomechanisms on the associated growth terms (i.e., first term on right hand side of Eq. (3) and Eq. (4)). Eq. (5)'s light attenuation model, based on the unidirectional illumination of the PBR in Fig. 1, was defined by Eq. (6) for the biomass production model (Eq. (3)), and Eq. (7) for the optical density model ((Eq. (4)). Light scattering phenomena is often reported to be significant in the presence of dense cell mass [25,26]. To overcome this, the embedded light attenuation model within the biomass model (Eq. (3)) included both the light absorption and light scattering terms. Only pigment dominated light absorption influences were therefore accounted for within the optical density model. These assumptions were concluded to be rational for a PBR of this size with a short light path length and low aeration rate (no visible gas bubbles during cultivation experiments). We therefore assumed light scattering induced by insignificant gas bubbles to be negligible in the models, especially for the optical density model.

$$I(z) = I_0 \cdot \exp[-(\tau \cdot X + \beta\ ) \cdot z] \tag{6}$$

$$I(z) = I_0 \cdot \exp[-(\tau \cdot \mathrm{OD}_{750}) \cdot z] \tag{7}$$

Where I_0 is the operational incident light intensity (µmol photons m^{-2} s^{-1}), z is the light path length (mm) and β is the light scattering coefficient (mm^{-1}). τ is the light attenuation coefficient with units of (mm^2 g^{-1}) and (mm^{-1}) for Eq. (6) and Eq. (7) respectively.

The simplified light attenuation model structures (i.e., Eq. (6) and Eq. (7)) have been reported by Anye Cho *et al*., [27] to be numerically stable for dynamic parameter estimation solvers without compromising the high solution accuracy, as compared to other literature complex light transmission models such as the two-flux approximation of the full radiation transfer equation [25,26]. However, incorporation of the PBR's cylindrical curvature effects in Eq. (6) and Eq. (7) will further increase the model complexity and computational burden for the dynamic parameter estimation solver. Therefore, further simplifications by approximating the observed circular cross-section with a rectangular cross-sectional area as reported in [27,28], and altering the light path length to 23.9 mm, was implemented.

When embedding Eq. (5), Eq. (6), Eq. (7) into Eq. (3) and Eq. (4), the overall predictive model is now a partial differential equation (PDE) due to the presence of both temporal and spatial dimensions, thus challenging to resolve both dimensions for the non-linear optimisation solver. To utilise a less complex ordinary differential equation (ODE) solver, a 20-step trapezoidal rule, as shown in Eq. (8), was employed to eliminate the spatial dimensions [15,19] in the model. Opposed to the commonly utilised 10-step trapezoidal rule in the literature [15,16,19], the extra number of trapezoidal steps were motivated by the observed higher magnitudes of biomass concentration (~ 5.3 g L^{-1} herein) and optical density (~ 24 herein) in PCC 11901 over that in the literature (< 3 g L^{-1}) [15,16] for slower growing cyanobacterial species. Therefore, the predictive models of PCC 11901 required more integration steps to better approximate its spatial dimension related parameters (i.e., u_m, k_s and k_i) during the parameter estimation process. Hence, Eqs. (6), (7), and (8) were then substituted into Eqs. (3) and (4) for the remainder of this study.

$$u\,(I) = \frac{u_m}{40} \cdot \sum_{n=1}^{19} \left(\frac{I_0}{I_0 + k_s + \frac{I_0^2}{k_i}} + \frac{2 \cdot I_{\frac{n \cdot L}{20}}}{I_{\frac{n \cdot L}{20}} + k_s + \frac{I_{\frac{n \cdot L}{20}}^2}{k_i}} + \frac{I_L}{I_L + k_s + \frac{I_L^2}{k_i}} \right) \tag{8}$$

2.4.3.2 Modelling PCC 6803 growth associated terms

Contrary to the statistically significant difference in PCC 11901, the final biomass and optical density datasets of PCC 6083 showed statistical insignificance (P>0.05) over the light intensity range (300 - 900 µmol photons m^{-2} s^{-1}) and was therefore not experiencing the above mentioned photomechanisms. However, upon performing dynamic student's *t*-test(s) over each state trajectory as discussed in Section 3.1, two to three discrete time points on each growth trajectory did show some level of statistical significance as seen in Fig. 2D, thereby implying a partial presence of these photomechanisms. Since these points were observed mostly around the exponential growth phase (i.e., between 20 and 60 hours), light saturation to a smaller extent was assumed present. Meanwhile, photoinhibition was completely ruled out (i.e., $\left[\frac{I(z)^2}{k_i}\right] \sim 0$ in Eq. (5)) as growth of PCC 6083 was not observed to decline over time and operational light intensities. However, the very small extent of light saturation implied that the influence of light attenuation on growth of PCC 6083 was also negligible (i.e., $\tau = \beta = 0$ in Eqs. (6) and (7)), thereby leading to Eq. (9). This resulting Monod-like model structure theoretically implies that the growth of PCC 6083 will increase linearly at lower operational light intensity until a saturation threshold is attained whereby the growth becomes maximal and independent of the operational light intensity. Herein, the former linear increase was assumed to only occur below 300 µmol photons m^{-2} s^{-1}, and the proposed model was therefore valid to simulate the saturating threshold (300 - 900 µmol photons m^{-2} s^{-1}) when embedding Eq. (9) into Eq. (3) and (4).

$$u\,(I) = u_m \cdot \frac{I_0}{I_0 + K_s} \tag{9}$$

Where K_s represent the light saturation (µmol photons m^{-2} s^{-1}).

2.5 Model parameter estimation methodology

To estimate the model parameters, a weighted non-linear least-square regression problem (see Eqs. (10a) to (10e)) was formulated. Due to the stiffness and high non-linearity of the proposed biomass and optical density models, orthogonal collocation over finite elements in time was utilised to numerically discretise the differential equations, thus transforming them into a series of non-linear algebraic equations. Thereafter, the resulting non-linear optimisation problem was solved with an interior point-based solver (i.e., IPOPT [29] version 3.11.1) through an open-source interface Pyomo [30,31] within the Python version 3.9 programming environment.

$$\min_{P} \Phi(\boldsymbol{p}) = \sum_{k=1}^{Nspp} \sum_{j=1}^{NV} \sum_{i=1}^{NP} \left(\frac{\hat{y}_{i,j,k} - y_{j,k}(t_i, \boldsymbol{p})}{\hat{y}_{i,j,k}} \right)^{\mathbf{2}} \cdot w_{i,j,k} \tag{10a}$$

Subject to:

$$\frac{d\boldsymbol{y}}{dt} = f(\boldsymbol{y}(t), p)\,, \qquad t \in [t_0, t_f] \tag{10b}$$

$$\boldsymbol{y_{lb}} \leq \boldsymbol{y} \leq \boldsymbol{y_{ub}} \tag{10c}$$

$$\boldsymbol{p_{lb}} \leq \boldsymbol{p} \leq \boldsymbol{p_{ub}} \tag{10d}$$

$$\boldsymbol{y}(t_0) = \boldsymbol{y_0} \tag{10e}$$

whereby $\boldsymbol{p}$ denotes a vector of parameters, $Nspp$, NV and NP are the number of species (i.e., PCC 11901 and PCC 6803), number of state variables (i.e. biomass concentration and optical density) and number of experimental data points, respectively, $\boldsymbol{y}$ denotes dynamic model output, $\hat{y}_{i,j,k}$ represents the experimental data point of species k with state variable j at time instant t_i, w_i is a weighting factor of species k for the data point of state variable j at time instant t_i, $\boldsymbol{y_{lb}}$, $\boldsymbol{y_{lb}}$, $\boldsymbol{p_{lb}}$ and $\boldsymbol{p_{ub}}$ denotes the lower and upper bounds of the state variables and

parameters, respectively, t_0 and t_f represents the initial and final cultivation times, $\boldsymbol{y_0}$ denotes the initial concentration of the state variables.

To simultaneously identify all model parameters as well as their confidence intervals, a bootstrapping technique was applied. This has increasingly been used in the machine learning community [32–34] for quantification of uncertainties. By implementing the bootstrapping methodology, the entire experimental dataset (i.e., 300 - 900 µmol photons m^{-2} s^{-1}) were repartitioned into PE1, PE2 and PE3 as illustrated in Table 2. Eqs. (10a) to (10e) were solved on every partition for dynamic model parameter estimation. The obtained parameter estimates were statistically aggregated by averaging for the mean and standard deviation. As a caveat, the upper and lower bounds of the experimental data sets (i.e., 300 and 900 µmol photons m^{-2} s^{-1}) were included in all three data partitions (Table 2). This was to guarantee the models high-fidelity extrapolations within the investigated range. This was later confirmed with a separate cross validation data set which was not utilised during parameter estimation (Table 2).

To evaluate the impact of the parameter confidence intervals on the various model prediction uncertainties, a Latin Hypercube Sampling methodology was used to draw 100 probabilistic samples from the confidence intervals. For each probabilistic sample, a dynamic model simulation was performed thereby amounting to a total of 100 Monte Carlo simulations whereby the mean prediction was computed and compared against the unseen experimental data sets. This implementation was carried out in Python version 3.9 using the *SMT* 1.0.0 and *Numpy* libraries.

3. Results and discussion

3.1 Evaluating the influence of light intensity on cyanobacterial growth

Cultures of PCC 11901 and PCC 6803 were grown at five different light intensities (300, 450, 600, 750 and 900 µmol photons m^{-2} s^{-1}), in order to investigate their growth dynamics over a wide range covering the low, medium, and high light intensities responsible for

photolimitation, photosaturation and photoinhibition respectively. Since the initial biomass concentrations and optical densities upon inoculation of the PBR were the same for all five investigated incident light intensities, the obtained final biomass concentrations and OD_{750nm} after 120 hrs of photoautotrophic growth were firstly analysed with student's *t*-test (P<0.05 being statistically significant) to identify the experimental light intensity (i.e., I_{0_opt}) that resulted in the highest biomass and OD_{750nm}. Thereafter, the entire biomass and OD_{750nm} time evolution profiles corresponding to I_{0_opt} were analysed with the remaining four data sets via a student's *t*-test (P<0.05 being statistically significant) for the effects of incident light intensity on the individual cyanobacterial strains.

The highest accumulation of biomass concentration and OD_{750nm} in PCC 11901 was observed at 750 µmol photons m^{-2} s^{-1} with corresponding values of 5.33 g DCW L^{-1} and OD_{750nm} = 24 (Fig. 2; Table 4). Biomass accumulation was similar between 300 to 600 µmol photons m^{-2} s^{-1}. From 750 to 900 µmol photons m^{-2} s^{-1}, biomass accumulation decreased by 24.6 % to 4.02 g DCW L^{-1}. A similar trend was observed in the OD_{750nm} measurements. The increase from 300/450/600 to 750 µmol photons m^{-2} s^{-1} suggests that cultivation of PCC 11901 below 750 µmol photons m^{-2} s^{-1} is suboptimal, possibly resulting in lower photosynthetic electron transport rates not sufficient for optimal carbon fixation [35].

Conversely, the decrease from 750 to 900 µmol photons m^{-2} s^{-1} could be due to photoinhibition [35], thus reducing the electron transport rate. It therefore confirms the use of Eq. (5) in Section 2.4.3 to mechanistically describe the three distinguishable photomechanisms, namely (i) photolimitation, (ii) photosaturation and (iii) photoinhibition. This further validates the implementation of the dynamic modelling approach to account for the dynamic light intensity effects on growth of PCC 11901. Fig. 2C shows the existence of statistical significance (P<0.05) over the entire trajectory and not just the final biomass concentration and OD_{750nm} in Fig. 2A.

The final biomass concentration and OD_{750nm} of PCC 6803 showed no statistically significant difference ($P > 0.05$) over the 300 to 900 µmol photons m^{-2} s^{-1} range (Fig. 2B). This was unexpected and could be due to the light intensity saturation threshold of PCC 6803 being lower than 300 µmol photons m^{-2} s^{-1}, which is when cultivation of PCC 6803 is typically performed [9]. However, the lack of declining growth due to photoinhibition within this 300 to 900 µmol photons m^{-2} s^{-1} range could be due to the light adaptation strategy outlined in Table 2. This may allow cells to acclimate to constant quantum yields, thus engendering similar rates of electron transport, even at the higher light intensities, and thus already at the theoretical maximum production rates of biomass and OD_{750nm} (Fig. 2B). However, it should be noted that this has not been observed in other studies [8–10], thus further experiments (e.g., fluorometry measurements [35,36]) to quantify electron transport should be conducted. This data could also be used to perform a Dynamic Flux Balance Analysis (DFBA) [37] which could lead to strategies for engineering the light absorption and light utilisation mechanisms of PCC 6803 in order to optimise this species for higher light intensities (i.e., >300 µmol photons m^{-2} s^{-1}) to achieve maximum titer and yields.

3.2 ~~Results of~~ M~~m~~athematical model-based analysis

Commented [AB4]: This addresses the comments of reviewer 2 regarding rephrasing the title.

3.2.1 Parameter estimation results

For the constructed dynamic models to yield reliable predictions of the observed biomass and optical density state variables, all model parameters must first be identified in a precise and accurate manner. Second, the estimated model parameters have associated uncertainties which, if known, can aid the model's predictions, allowing fidelities to be assessed and enabling the implementation for bioprocess control and optimisation. The bootstrapping technique is often utilised for this uncertainty quantification in machine learning models [32,33,38] and was herein adapted for this analysis, as discussed in Section 2.5. Table 3 lists the identified mean

parameter values for *n*=3 bootstrapping partitions and their standard deviations for both the optical density and biomass models respectively. These parameter results were compared against those available from previous studies as seen in the last column of Table 3, showing that they were well within the range from previous studies [10,16,17,22,23,39]. The sole exception was for the OD light absorption coefficient which was previously unavailable and therefore compared against those from previous literature biomass models [22,23], which generally agreed with our outcomes and thereby validated the reliability of the presented results.

Figure 3 and 4 show the predicted biomass model fit against the experimental data points from which the optimal parameter results in Table 3 were obtained via the bootstrapping technique. The fittings of the biomass and $\mathrm{OD}_{750\mathrm{nm}}$ models were similar as justified by their equally obtained percentage relative errors (%RE) (i.e., circa 13.8 % and 18.0 % for PCC 11901 and PCC 6803). Therefore, only the biomass model fittings were shown herein while the $\mathrm{OD}_{750\mathrm{nm}}$ model fittings were presented in Figs. S1 and S2. An in depth analysis of the model fitting results were carried out by computing the overall average percentage relative errors (%RE), which showed the model predictions of PCC 11901 (i.e., 13.8 %) to follow the experimental datasets better than the one of PCC 6803 (i.e., 18.0 %), with similar observations for the cross validation runs (i.e., 9.3% and 18.8 % respectively). Whilst this was expected due to the larger standard deviation between the experimental datasets observed in PCC 6803 (Fig. 4 and Fig. S2), it was deemed acceptable when considering that typical light driven bioprocesses are often associated with larger uncertainties [27,40]. Nonetheless, all the model trajectories were seen to represent the experimental data points, thereby capturing the underlying complex behaviours with a small subset of biokinetic parameters. This confirms that the postulated mechanistic hypothesis during the model construction and implemented model structural simplifications for the dynamic parameter estimation solver were all valid.

3.2.2 Probabilistic model predictive validations

To utilise the constructed dynamic models for estimating the optimal operating conditions for industrial use of strains, as well as for model implementation during long-term bioprocess simulation, optimisation and control, it was necessary to evaluate the model performances for predicting unseen experimental data sets. Since the experimental data sets at 450, 600 and 750 μmol photons m^{-2} s^{-1} represented the cross validation runs in Table 2 and without embedded uncertainties, the same conditions were simulated upon embedding the aggregated bootstrapping uncertainties. For this, 100 Monte Carlo simulations were performed by sampling the model parameter confidence intervals in Table 3 and propagating their influences on the dynamic model's output. Fig. 5 shows the biomass model predictions under uncertainty for the two cyanobacterial strains. The mean prediction from the uncertainty bands (in grey) were computed to compare against the experimental data points. Whilst the uncertainty bands reflect the degree of variability imposed by the parameter confidence intervals, those for the biomass and optical density models were similar. Thus, only those for the biomass model were shown in Fig. 5 while those of the optical density models are presented in Fig. S3. These uncertainty bands are observed to grow (i.e., increase of bandwidth size) with time, indicating the models to be responsive to changes of these parameters. Generally, as the parameter changes did not induce large uncertainty bands, they are therefore safe for re-estimation during online dynamic bioprocess control. To evaluate the model's prediction under uncertainty versus the pure model outputs, the overall %RE in Fig. 5 were computed (i.e., 8.9 % and 19.4 % for PCC 11901 and PCC 6803 respectively) and compared to that of the bootstrapping cross validation runs (i.e., 9.3 % and 18.8 % for PCC 11901 and PCC 6803 respectively). From this analysis, a 4.5 % prediction improvement in PCC 11901 and 3.1 % prediction deterioration in PCC 6803, respectively, were observed under uncertainty. The former percentage improvement was expected for the two models (i.e., PCC 11901 and PCC 6803) as mildly

perturbing responsive model parameters have been shown by Anye Cho *et al*., [27] to improve prediction accuracy. However, the unexpected prediction deterioration in PCC 6803 can be attributed to its noisy experimental data sets. Hence, the small 3.1 % prediction deterioration is expected to be reversed if presented with a less noisy experimental data sets since the simulation performance will be relatively high.

3.2.3 Overall comparison of the two cyanobacterial strains

As the prediction performance of the dynamic models for both the seen and the cross validated experimental datasets were within the wide operating range from 300 to 900 μmol photons m^{-2} s^{-1} , its full potential was then explored to address pertinent questions about the bioprocess dynamics, in particular: (i) which of the two cyanobacterial strains is fastest growing across a range of light intensities, (ii) what are their respective optimal light intensities, and (iii) does light intensity impact their upscaling potentials?

From the growth characteristics of the two strains outlined in Table 3, it was observed that the maximum specific growth rate of PCC 91101 was over two fold higher than that of PCC 6803. Whilst this increase was consistent with the experimental data sets, the order of magnitude was however about four-fold higher when comparing the final biomass concentration and optical densities as illustrated in Table 4. These disparities indicate that the results outlined in Table 4 are insufficient for characterising the strain specific growth properties as the dynamic model and estimated parameters can predict these results, but the reverse is not possible. Nonetheless, the faster growth of PCC 11901 agrees with previous studies [8,10], which demonstrated that it was superior to other 'fast' growing cyanobacterial strains like UTEX 2973 and PCC 7002. The light saturation coefficient of PCC 6803 was about two-fold lower than that of PCC 11901, indicating superior light affinity and utilisation efficiency. This implies PCC 6803 should be the faster growing strain which contradicts previous literature findings [8,10]. Explaining this

inconsistency is far beyond the capabilities of the linearised curve fitting literature methods for estimating and comparing maximum specific growth rate. This was addressed with the dynamic mechanistic modelling approach by analysing the maximum specific growth and decay rates in Table 3. Those of PCC 6803 were seen to be of similar order of magnitudes while the decay rate of PCC 11901 was about 67-fold lower than its maximum specific growth rate. This implies that for the portion of absorbed and utilised light intensities within the 300 to 900 µmol photons m^{-2} s^{-1} range, PCC 11901 was experiencing unbalanced growth dominating Eqs. (3) and (4), whereas that of PCC 6803 was balanced. Hence, the higher light affinity and utilisation efficiency of PCC 6803 compared to PCC 11901 was not directed towards growth promoting activities and was herein interpreted to be either for (i) cell maintenance, and/or (ii) fluorescence heat generation. Cell maintenance encompasses non-growth related metabolic activities performed by the cells to stay alive which usually consume energy in the form of adenosine triphosphate (ATP). Since ATP and nicotinamide adenine dinucleotide phosphate (NADPH) are the products of light dependent reactions [41], it was reasonable to assume that ATP and NADPH generation in PCC 6803 was mostly directed towards cell maintenance and not for carbon fixation via Calvin-Benson-Basshan cycle. This assumption was reasonably valid as the final biomass concentration ultimately derived from carbon fixation did not change within the investigated 300 to 900 µmol photons m^{-2} s^{-1} range. This also suggests that extra absorbed light above 300 µmol photons m^{-2} s^{-1} was mostly wasted as heat and not utilised for growth of PCC 6803 since Eqs. (3) and (4) were balanced.

The remaining two questions were only valid for PCC 11901 since the 300 to 900 µmol photons m^{-2} s^{-1} range were observed to be above the light intensity saturation threshold for PCC 6803, suggesting growth is light independent. As per the optimal light intensity of PCC 11901, the model derivative with respective to the light intensity was taken and equated to zero (i.e., $\frac{d\mu(I)}{dI} = 0$), thereby resulting in optimal light intensities, $I_{opt} = \sqrt{k_s \cdot k_I}$ of 727.0 µmol photons

m^{-2} s^{-1} and 742.9 µmol photons m^{-2} s^{-1} for the respective biomass and optical density models, respectively, and averaging 735.0 µmol photons m^{-2} s^{-1} to encompass both aspects. The similar I_{opt} values between both models (i.e., biomass and OD_{750nm}) suggest that they can be used interchangeably for (i) optimal design of experiments, and (ii) online bioprocess control since OD_{750nm} measurements with a UV/VIS spectrophotometer are more easily obtained over quantifying biomass. Second, these predicted optimal values are within the range of several other cyanobacterial species [8,10,42], supporting their validity. Although I_{opt} was slightly lower than the optimal 750.0 µmol photons m^{-2} s^{-1} reported highest biomass and OD_{750nm} from experimental data (i.e., I_{0_opt}), the 15 µmol photons m^{-2} s^{-1} difference was negligibly small (circa 2 %) and indicates the accurate dynamic estimation of k_s and k_I under the PBR light path length with 20-step trapezoidal approximations.

Next, we considered whether the upscaling potential of PCC 11901 will be severely impacted by light intensity. The light absorption coefficient was identified as the main parameter to be compared against values from photobioreactors of different scales and configurations. This was motivated by the intrinsic nature of the light absorption coefficient to cyanobacteria and the light attenuation challenges being the primary limitation for upscaling photobiological processes, as was investigated by Anye Cho *et al.*, [19]. Therefore, a high light absorption coefficient would indicate rapid diminishing local light transmissions within the PBR as its diameter was increased for upscaling, and vice-versa. The PCC 11901 light absorption coefficient compared well to that observed in previous studies [22,23] (i.e., $67 \leq \tau \leq 225$ mm^2 g^{-1}) outlined in Table 3. This suggests that upscaling of PCC 11901 cultivation will not be severely impacted by light intensity since previous studies used PBRs ranging from 0.5 L cylindrical PBRs [43,44], 1.0 L flat-plate [21,23] and tubular [45] PBRs, to as large as 120.0 L flat-plate PBRs [46,47].

4. Conclusions

In this investigation, experimental observation of biomass concentrations and optical densities, and statistical analysis with student's *t*-test were jointly exploited to support the incorporation of various photomechanisms within the dynamic mechanistic models of two cyanobacterial strains: PCC 11901 and PCC 6803. Whilst such models for OD_{750nm} were previously unavailable, the similarities of their growth profile to biomass models justified the existence of similar model structures and was herein implemented for the first time. Even so, the model for PCC 11901 embedded the complicated influences of incident light intensity, light attenuation and photomechanisms, whereas the one for PCC 6803 was only limited by the incident light intensity and photosaturation mechanisms. To simultaneously estimate the model parameter values and their associated confidence intervals, bootstrapping techniques with 3-fold cross validations was implemented. Thereafter, the models' predictions under uncertainties were thoroughly validated against unseen experimental data sets with small simulation errors averaging less than 19 %. Of the two species, PCC 11901 showed superior prediction fidelities and faster growth. Whilst fluorometry measurements are recommended in future for confirming the light-stressed photosynthetic activities of PCC 6803 within the 300 to 900 µmol photons m^{-2} s^{-1} range, further model-based analysis was carried out on the PCC 11901 model parameters. As a result, 735.0 µmol photons m^{-2} s^{-1} was identified as the optimal cultivation light intensity, and without severe light limitations during bioprocess upscaling. Therefore, these presented findings will benefit future biotechnological upscaling, online bioprocess control and exploitation of these strains.

Acknowledgement

B.A.C. acknowledges funding from the Commonwealth Scholarship Commission, United Kingdom. J.A.M.C. acknowledges funding support from a FEBS short term fellowship and University of Cordoba fellowship. L.A.M. acknowledge funding support from the BBSRC Norwich Research Park Doctoral Training Partnership program (grant number BB/S507404/1).

References

[1] Lindberg P, Park S, Melis A. Engineering a platform for photosynthetic isoprene production in cyanobacteria, using Synechocystis as the model organism. Metab Eng 2010;12:70–9. https://doi.org/10.1016/j.ymben.2009.10.001.

[2] Niederholtmeyer H, Wolfstädter BT, Savage DF, Silver PA, Way JC. Engineering cyanobacteria to synthesize and export hydrophilic products. Appl Environ Microbiol 2010;76:3462–6. https://doi.org/10.1128/AEM.00202-10.

[3] Balskus EP, Walsh CT. The Genetic and Molecular Basis for Sunscreen Biosynthesis in Cyanobacteria. Science (1979) 2010;329:1653–6. https://doi.org/10.1126/science.1193637.

[4] Brilisauer K, Rapp J, Rath P, Schöllhorn A, Bleul L, Weiß E, et al. Cyanobacterial antimetabolite 7-deoxy-sedoheptulose blocks the shikimate pathway to inhibit the growth of prototrophic organisms. Nat Commun 2019;10. https://doi.org/10.1038/s41467-019-08476-8.

[5] Pilon L, Berberoğlu H, Kandilian R. Radiation transfer in photobiological carbon dioxide fixation and fuel production by microalgae. J Quant Spectrosc Radiat Transf 2011;112:2639–60. https://doi.org/10.1016/j.jqsrt.2011.07.004.

[6] Collotta M, Champagne P, Mabee W, Tomasoni G. Wastewater and waste CO2 for sustainable biofuels from microalgae. Algal Res 2018;29:12–21. https://doi.org/10.1016/j.algal.2017.11.013.

[7] Roh H, Lee JS, Choi H il, Sung YJ, Choi SY, Woo HM, et al. Improved CO2-derived polyhydroxybutyrate (PHB) production by engineering fast-growing cyanobacterium

Synechococcus elongatus UTEX 2973 for potential utilization of flue gas. Bioresour Technol 2021;327:124789. https://doi.org/10.1016/j.biortech.2021.124789.

[8] Mills LA, Moreno-Cabezuelo JÁ, Włodarczyk A, Victoria AJ, Mejías R, Nenninger A, et al. Development of a Biotechnology Platform for the Fast-Growing Cyanobacterium Synechococcus sp. PCC 11901. Biomolecules 2022;12:872. https://doi.org/10.3390/biom12070872.

[9] Yu J, Liberton M, Cliften PF, Head RD, Jacobs JM, Smith RD, et al. Synechococcus elongatus UTEX 2973, a fast growing cyanobacterial chassis for biosynthesis using light and CO_2 . Sci Rep 2015;5:8132. https://doi.org/10.1038/srep08132.

[10] Włodarczyk A, Selão TT, Norling B, Nixon PJ. Newly discovered Synechococcus sp. PCC 11901 is a robust cyanobacterial strain for high biomass production. Commun Biol 2020;3. https://doi.org/10.1038/s42003-020-0910-8.

[11] Clark RL, McGinley LL, Purdy HM, Korosh TC, Reed JL, Root TW, et al. Light-optimized growth of cyanobacterial cultures: Growth phases and productivity of biomass and secreted molecules in light-limited batch growth. Metab Eng 2018;47:230–42. https://doi.org/10.1016/j.ymben.2018.03.017.

[12] Jaiswal D, Sengupta A, Sohoni S, Sengupta S, Phadnavis AG, Pakrasi HB, et al. Genome Features and Biochemical Characteristics of a Robust, Fast Growing and Naturally Transformable Cyanobacterium Synechococcus elongatus PCC 11801 Isolated from India. Sci Rep 2018;8:1–13. https://doi.org/10.1038/s41598-018-34872-z.

[13] Lea-Smith DJ, Vasudevan R, Howe CJ. Generation of marked and markerless mutants in model cyanobacterial species. Journal of Visualized Experiments 2016;2016:1–12. https://doi.org/10.3791/54001.

[14] Snoep JL, Mrwebi M, Schuurmans JM, Rohwer JM, Teixeira de Mattor MJT. Control of specific growth rate in Saccharomyces cerevisiae. Microbiology (N Y) 2009;155:1699–707. https://doi.org/10.1099/mic.0.023119-0.

[15] Zhang D, Dechatiwongse P, Del-Rio-Chanona EA, Hellgardt K, Maitland GC, Vassiliadis VS. Analysis of the cyanobacterial hydrogen photoproduction process via model identification and process simulation. Chem Eng Sci 2015;128:130–46. https://doi.org/10.1016/j.ces.2015.01.059.

[16] del Rio-Chanona EA, Dechatiwongse P, Zhang D, Maitland GC, Hellgardt K, Arellano-Garcia H, et al. Optimal Operation Strategy for Biohydrogen Production. Ind Eng Chem Res 2015;54:6334–43. https://doi.org/10.1021/acs.iecr.5b00612.

[17] Dechatiwongse P, Srisamai S, Maitland G, Hellgardt K. Effects of light and temperature on the photoautotrophic growth and photoinhibition of nitrogen-fixing cyanobacterium Cyanothece sp. ATCC 51142. Algal Res 2014;5:103–11. https://doi.org/10.1016/j.algal.2014.06.004.

[18] Lea-Smith DJ, Bombelli P, Dennis JS, Scott SA, Smith AG, Howe CJ. Phycobilisome-deficient strains of synechocystis sp. PCC 6803 have reduced size and require carbon-limiting conditions to exhibit enhanced productivity. Plant Physiol 2014;165:705–14. https://doi.org/10.1104/pp.114.237206.

[19] Anye Cho B, Carvalho Servia MÁ, del Río Chanona EA, Smith R, Zhang D. Synergising biomass growth kinetics and transport mechanisms to simulate light/dark cycle effects on photo- production systems. Biotechnol Bioeng 2021;118:1932–42. https://doi.org/10.1002/bit.27707.

[20] Cordara A, Re A, Pagliano C, van Alphen P, Pirone R, Saracco G, et al. Analysis of the light intensity dependence of the growth of Synechocystis and of the light

distribution in a photobioreactor energized by 635 nm light. PeerJ 2018;2018:1–28. https://doi.org/10.7717/peerj.5256.

[21] Zhang D, Dechatiwongse P, Hellgardt K. Modelling light transmission , cyanobacterial growth kinetics and fl uid dynamics in a laboratory scale multiphase photo-bioreactor for biological hydrogen production. Algal Res 2015;8:99–107. https://doi.org/10.1016/j.algal.2015.01.006.

[22] Zhang D, Dechatiwongse P, del Rio-Chanona EA, Maitland GC, Hellgardt K, Vassiliadis VS. Dynamic modelling of high biomass density cultivation and biohydrogen production in different scales of flat plate photobioreactors. Biotechnol Bioeng 2015;112:2429–38. https://doi.org/10.1002/bit.25661.

[23] Zhang D, Dechatiwongse P, del Rio-Chanona EA, Maitland GC, Hellgardt K, Vassiliadis VS. Modelling of light and temperature influences on cyanobacterial growth and biohydrogen production. Algal Res 2015;9:263–74. https://doi.org/10.1016/j.algal.2015.03.015.

[24] Williams JGK. Construction of Specific Mutations in Photosystem II Photosynthetic Reaction Center by Genetic Engineering Methods in Synechocystis 6803. Methods Enzymol 1988;167:766–78. https://doi.org/10.1016/0076-6879(88)67088-1.

[25] Cornet JF, Dussap CG, Gros JB, Binois C, Lasseur C. A simplified monodimensional approach for modeling coupling between radiant light transfer and growth kinetics in photobioreactors. Chem Eng Sci 1995;50:1489–500. https://doi.org/10.1016/0009-2509(95)00022-W.

[26] Pottier L, Pruvost J, Deremetz J, Cornet J-F, Legrand J, Dussap CG. A fully predictive model for one-dimensional light attenuation byChlamydomonas reinhardtii in a torus

photobioreactor. Biotechnol Bioeng 2005;91:569–82. https://doi.org/10.1002/bit.20475.

[27] Anye Cho B, Ross BS, du Toit JP, Pott RWMC, del Río Chanona EA, Zhang D. Dynamic modelling of Rhodopseudomonas palustris biohydrogen production: Perturbation analysis and photobioreactor upscaling. Int J Hydrogen Energy 2021;46:36696–708. https://doi.org/10.1016/j.ijhydene.2021.08.162.

[28] Palamae S, Choorit W, Dechatiwongse P, Zhang D, Antonio del Rio-Chanona E, Chisti Y. Production of renewable biohydrogen by Rhodobacter sphaeroides S10: A comparison of photobioreactors. J Clean Prod 2018;181:318–28. https://doi.org/10.1016/j.jclepro.2018.01.238.

[29] Wächter A, Biegler LT. On the implementation of an interior-point filter line-search algorithm for large-scale nonlinear programming. Math Program 2006;106:25–57. https://doi.org/10.1007/s10107-004-0559-y.

[30] Nicholson B, Siirola JD, Watson JP, Zavala VM, Biegler LT. Pyomo.Dae: a Modeling and Automatic Discretization Framework for Optimization With Differential and Algebraic Equations. Math Program Comput 2018;10:187–223. https://doi.org/10.1007/s12532-017-0127-0.

[31] Hart WE, Laird C, Watson J-P, Woodruff DL. Pyomo – Optimization Modeling in Python. vol. 67. Boston, MA: Springer US; 2012. https://doi.org/10.1007/978-1-4614-3226-5.

[32] Mowbray M, Savage T, Wu C, Song Z, Cho BA, del Rio-Chanona EA, et al. Machine learning for biochemical engineering: A review. Biochem Eng J 2021;172:108054. https://doi.org/10.1016/j.bej.2021.108054.

[33] Rogers AW, Vega-Ramon F, Yan J, del Río-Chanona EA, Jing K, Zhang D. A transfer learning approach for predictive modeling of bioprocesses using small data. Biotechnol Bioeng 2022;119:411–22. https://doi.org/10.1002/bit.27980.

[34] Pinto J, de Azevedo CR, Oliveira R, von Stosch M. A bootstrap-aggregated hybrid semi-parametric modeling framework for bioprocess development. Bioprocess Biosyst Eng 2019;42:1853–65. https://doi.org/10.1007/s00449-019-02181-y.

[35] Tyystja¨rvi ET, Hakala M, Sarvikas P. Mathematical modelling of the light response curve of photoinhibition of Photosystem II. n.d.

[36] Baker NR. Chlorophyll fluorescence: A probe of photosynthesis in vivo. Annu Rev Plant Biol 2008;59:89–113. https://doi.org/10.1146/annurev.arplant.59.032607.092759.

[37] Gerken-Starepravo L, Zhu X, Cho BA, Vega-Ramon F, Pennington O, Antonio del Río-Chanona E, et al. An MIQP framework for metabolic pathways optimisation and dynamic flux analysis. Digital Chemical Engineering 2022;2:100011. https://doi.org/10.1016/j.dche.2022.100011.

[38] Pinto J, de Azevedo CR, Oliveira R, von Stosch M. A bootstrap-aggregated hybrid semi-parametric modeling framework for bioprocess development. Bioprocess Biosyst Eng 2019;42:1853–65. https://doi.org/10.1007/s00449-019-02181-y.

[39] Cabello J, Morales M, Revah S. Dynamic photosynthetic response of the microalga Scenedesmus obtusiusculus to light intensity perturbations. Chemical Engineering Journal 2014;252:104–11. https://doi.org/10.1016/j.cej.2014.04.073.

[40] Sadino-Riquelme MC, Rivas J, Jeison D, Hayes RE, Donoso-Bravo A. Making sense of parameter estimation and model simulation in bioprocesses. Biotechnol Bioeng 2020;117:1357–66. https://doi.org/10.1002/bit.27294.

[41] Carvalho AP, Silva SO, Baptista JM, Malcata FX. Light requirements in microalgal photobioreactors: An overview of biophotonic aspects. Appl Microbiol Biotechnol 2011;89:1275–88. https://doi.org/10.1007/s00253-010-3047-8.

[42] Salleh SF, Kamaruddin A, Uzir MH, Mohamed AR, Shamsuddin AH. Modeling the light attenuation phenomenon during photoautotrophic growth of A. variabilis ATCC 29413 in a batch photobioreactor. Journal of Chemical Technology and Biotechnology 2017;92:358–66. https://doi.org/10.1002/jctb.5013.

[43] Rivera C, Niño L, Gelves G. Modeling of phycocyanin production from Spirulina platensis using different light-emitting diodes. S Afr J Chem Eng 2021;37:167–78. https://doi.org/10.1016/j.sajce.2021.05.005.

[44] del Rio-Chanona EA, Liu J, Wagner JL, Zhang D, Meng Y, Xue S, et al. Dynamic modeling of green algae cultivation in a photobioreactor for sustainable biodiesel production. Biotechnol Bioeng 2018;115:359–70. https://doi.org/10.1002/bit.26483.

[45] Rio-chanona EA, Ahmed N rashid, Zhang D, Lu Y, Jing K. Kinetic Modeling and Process Analysis for Desmodesmus sp. Lutein Photo-Production. AICHE Journal 2017;63:2546–54. https://doi.org/10.1002/aic.

[46] del Rio-Chanona EA, Wagner JL, Ali H, Fiorelli F, Zhang D, Hellgardt K. Deep learning-based surrogate modeling and optimization for microalgal biofuel production and photobioreactor design. AIChE Journal 2019;65:915–23. https://doi.org/https://doi.org/10.1002/aic.16473.

[47] Ali H, Solsvik J, Wagner JL, Zhang D, Hellgardt K, Park CW. CFD and kinetic- based modeling to optimize the sparger design of a large- scale photobioreactor for scaling up of biofuel production. Biotechnol Bioeng 2019;116:2200–11. https://doi.org/10.1002/bit.27010.

Response to all reviewers' comments

Firstly, we would like to thank all the reviewers for their insightful comments and constructive suggestions, which helps to improve the quality of this manuscript. Hence, our responses are as follows:

Response to Reviewer 1

The paper titled "Integrated experimental and photo-mechanistic modelling of biomass and optical density production for the cyanobacterium Synechococcus sp. PCC 11901" focuses on the development and validation of a procedure to predict the growth of two different microalgae strains. The title must be thus modified. The procedure provides is quite regular, thus it consists of the definition of equations relating to the most relevant parameters influencing the growth of microalgae, such as light and biomass concentration/optical density. The use of differential equations allows consider the variation of culture parameters with time, but in this case, fixed values of characteristics parameters were considered. This is a regular strategy generally accepted. The results provided are of interest but the novelty and relevance of the work are not high.

Response: Thank you for the positive attitude towards our work and for suggesting a change of the paper title. Even though we investigated two cyanobacterial strains, the emphasis was on the fastest growing cyanobacterium identified to date, *Synechococcus* sp. PCC 11901. Nonetheless, we have retitled the paper to "Integrated experimental and photo-mechanistic modelling of biomass and optical density production of fast versus slow growing model cyanobacteria". Hopefully this new title attracts a wider audience and informs them of the current advancements in cyanobacterial biotechnology.

Response to Reviewer 2

In this submitted manuscript, the Authors present a study of both experimental and modeling of the kinetic of biomass growth and optical density for the cyanobacterium *Synechococcus* sp. PCC 11901, which is recognized as "fastest growing cyanobacterium identified to date" species and compared to another strain *Synechocystis* sp. PCC 6803. Particular attention was given to the light attenuation effects and photomechanisms (i.e., photolimitation, photosaturation and photoinhibition) over the growth kinetics of both strains.

The topic of light effects over the kinetic growth is quite relevant, particularly given the scale-up drawbacks, hence it is worthy of investigating. Overall, the manuscript is well-written and organized and used adequate scientific methodology. Also, the mathematical model approach, which consists in a distributed parameter mechanistic model is very robust and reliable. The Authors provided a parallel analysis of kinetic modeling of biomass growth and optical density (OD750nm) and were able to investigate the photo-mechanistic influences and adequately describe the experimental data. The OD750 kinetic model results were proved to have similar results when compared to the biomass, what is a practical advantage since it is an easier method to quantify biomass.

The Authors also provided satisfactorily results of validation of the modeling through independent experimental data, hence showed that the model has predictive capacity. Those results strongly contribute for scale-up purposes. Finally, the Authors provided in-depth mechanistic discussion. Therefore, the manuscript brings novelty and contributions to the field. Overall, the paper presents enough novelty and findings, so in my perspective is worthy of consideration for publication. However, before that, some issues (as listed below) must be addressed or answered. If the Authors are willing to address them, I would be favourable for the manuscript publication.

In this sense, after a careful reading of the manuscript, based on the above-mentioned (and on the specific comments below), I would recommend the publication of the manuscript in the Algal Research journal, after the issues are overcome.

Major Issues

1) (2.3 Analytical methods) Are Eq. (1) and (2) really necessary? Maybe they could be provided in Sup. Material.

Response: Thank you for suggesting this. As you have noted, the manuscript blends both experimental and modelling approaches. Therefore, we find Eqs. (1) and (2) to complement the experimental methodology section of the manuscript and improves the readership. Hence, we would like to retain them within the main text rather than in the supplementary material section.

2) (Eq. 5) Authors applied Aiba model structure, please provide more details for this model use and assumptions.

Response: Thank you for recommending this. We agree and have now added a few lines "Under low light intensities, growth rate increases linearly with increasing light intensity till saturation at the optimal light intensity. Beyond this, the growth rate decreases with further increase in the light intensity." in the revised version of the manuscript.

3) (p. 11) It is quite plausible to assume a rectangular cross-sectional area instead of a circular cross-section, as a simplifying hypothesis, however why did the Authors alter the light path length to 23.9 mm? (They reported that the internal diameter of of the PBR was 27 mm).

Response: Yes, this is correct. In equating the two cross-sectional areas (i.e., rectangular cross-sectional area = circular cross-section area), the diameter of the rectangular cross-sectional area becomes an unknown variable to be identified. Solving for the diameter by rearranging the equation results to 23.9 mm and this is described in the cited references within the manuscript.

4) (p. 11) The Authors state "To utilise a less complex ordinary differential equation (ODE) solver, a 20-step trapezoidal rule, as shown in Eq. (8), was employed to eliminate the spatial dimensions [15,19] in the model. Opposed to the commonly utilised 10-step trapezoidal rule in the literature [15,16,19],…". Is quite strange to compare the use of 20 steps in the discretization instead of 10 steps, commonly, reported in the literature (as stated by the Authors). This is a typical problem of accuracy vs. computation effort. The use of more or less discretization steps depends on particular data/system and must be considered accordingly. Even studies to evaluate how many discretization steps are necessary can be performed, since sometimes despite their increase no substantial increase in the results quality is achieved. Did, in this case, the 20-step discretization achieved better values?

Response: Thank you for asking this. The strain's biomass concentration is the main indicator of the number steps to be employed in the trapezoidal rules due to light attenuation by cellular absorption. Therefore, faster growing strains will require more steps to accurately approximate the specific growth over the light transmission direction. So, the choice of 20-step herein over 10-step in the literature was due to the strain accumulating over two times (~ 5.3 g L^{-1}) more biomass than the literature strain (< 3 g L^{-1}). Whilst 10-step will yield inferior results, 20-step trapezoidal rule will certainly yield results of better quality. Hence, we chose the better-quality result with the 20-step trapezoidal rule.

5) (3.2 Results of mathematical model-based analysis) It is already in Results and discussion section, no need of "Results of" in the Section title.

Response: Thank you for raising this ambiguity. We agree and have now paraphrased the title to "mathematical model-based analysis" in the revised version of the manuscript.

6) Figure 4B, what is the reason for the peak of biomass around of 60 hours and its subsequent decrease? (Similar behavior happens to other data). (Conclusions) Since the Authors concluded that "As a result, 735.0 µmol photons m-2 s-1 was identified as the optimal cultivation light intensity, and without severe light limitations during bioprocess upscaling. Therefore, these presented findings will benefit future biotechnological upscaling, online bioprocess control and exploitation of these strains.", and also the model is a distributed-parameter model (light attenuation model). The Authors are encouraged to provide, at least in the optimal condition, the values and/or profile of light intensity as a function of the PBR length, this analysis may contribute to the upscaling of the process.

Response: Thank you for asking this. We reported the optimal light intensity as 735.0 µmol photons m^{-2} s^{-1} for PCC 11901 in section 3.2.3. However, no optimal light intensity was identified for PCC 6803 since the lower bound (i.e., 300 µmol photons m^{-2} s^{-1}) was already far above the strain's saturation light intensity, thus independent of light intensity as discussed in section 3.2.3.

Minor Issues

Some language issues (grammar, typos, punctuation etc) must be addressed, for instance: (i) (p. 7, line 26) "deionise water"

Response: Thank you for recommending this. We have now paraphrased this to “deionised water” in the revised version of the manuscript.

(ii) (p. 8, 9) "t- test(s)"

Response: Thank you for highlighting this. We think this is not a typo as the sentence is communicating that many t-test we performed as indicated by (s). Therefore, we have not modified the sentence.

(iii) (Table 4) Provide units (Biomass concentration)

Response: Thank you for recommending this. We agree and have now included the units in the revised version of the manuscript

(iv) Units (please revise)

Response: Thank you for asking this. This has been checked in the revised version of the manuscript.

Highlights (3-5 bullet points):

- Dynamic photo-mechanistic interpretations of cyanobacterial bioconversion rates.
- Experimental and statistical analysis to inform photo-mechanistic influences.
- Similar model structures for biomass growth and optical density accumulation.
- 735.0 μmol photons m^{-2} s^{-1} optimal light intensity for *Synechococcus* sp. PCC 11901.
- Over two-fold faster growth for PCC 11901 versus PCC 6803 at all light intensities.

Graphical Abstract

Graphical abstract

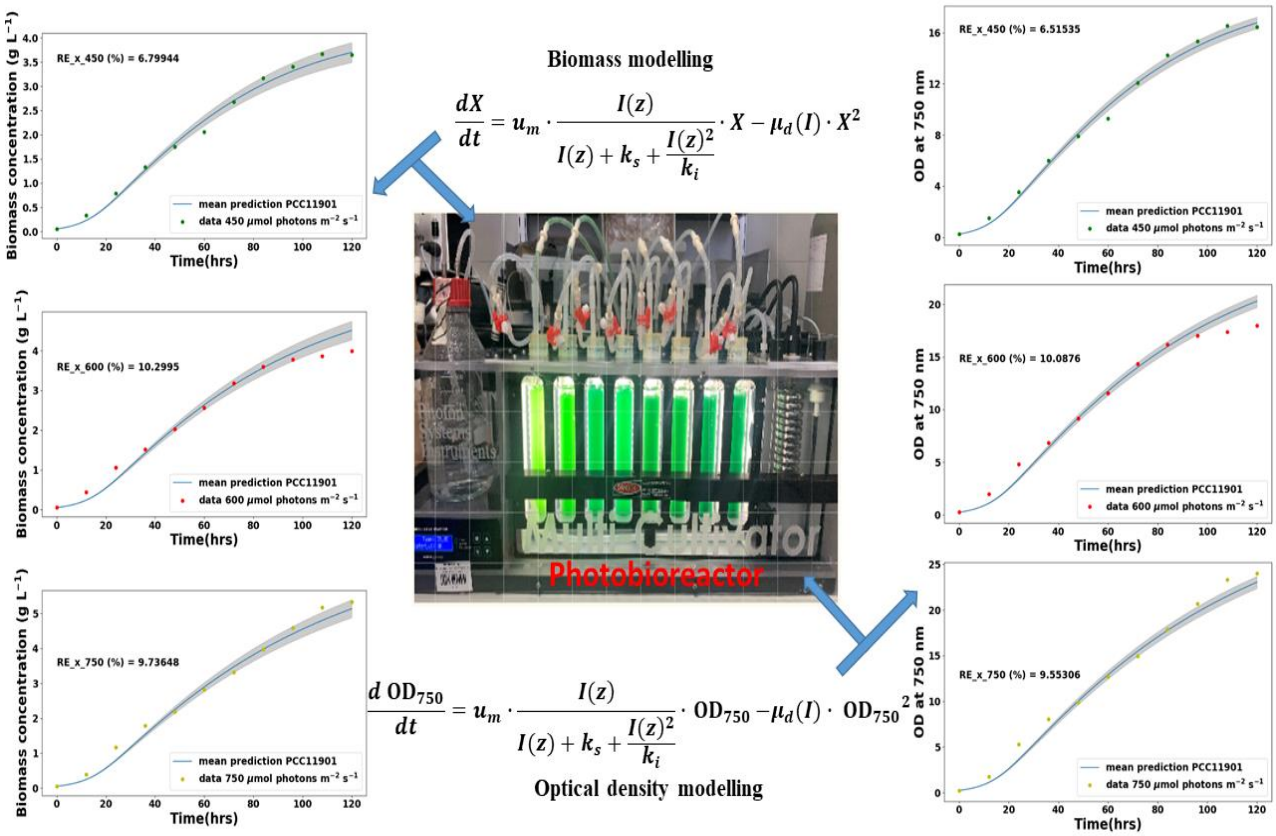

List of Figures

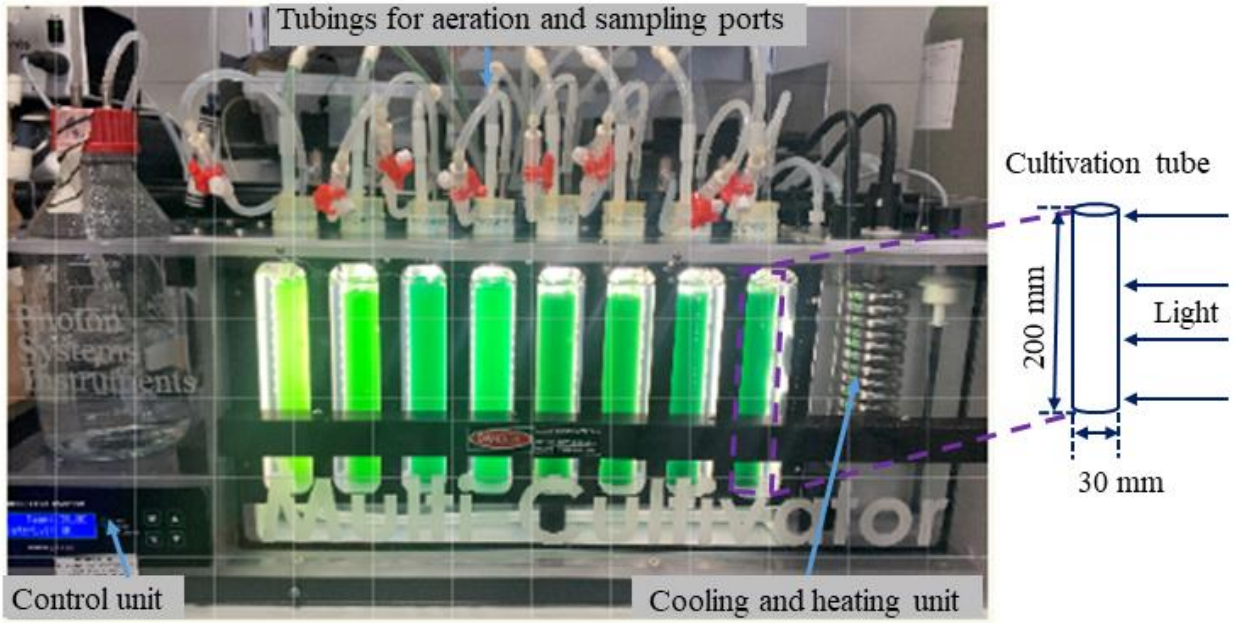

Figure 1: MC-1000 multicultivator bioreactor setup (Photon Systems Instruments, Czech Republic).

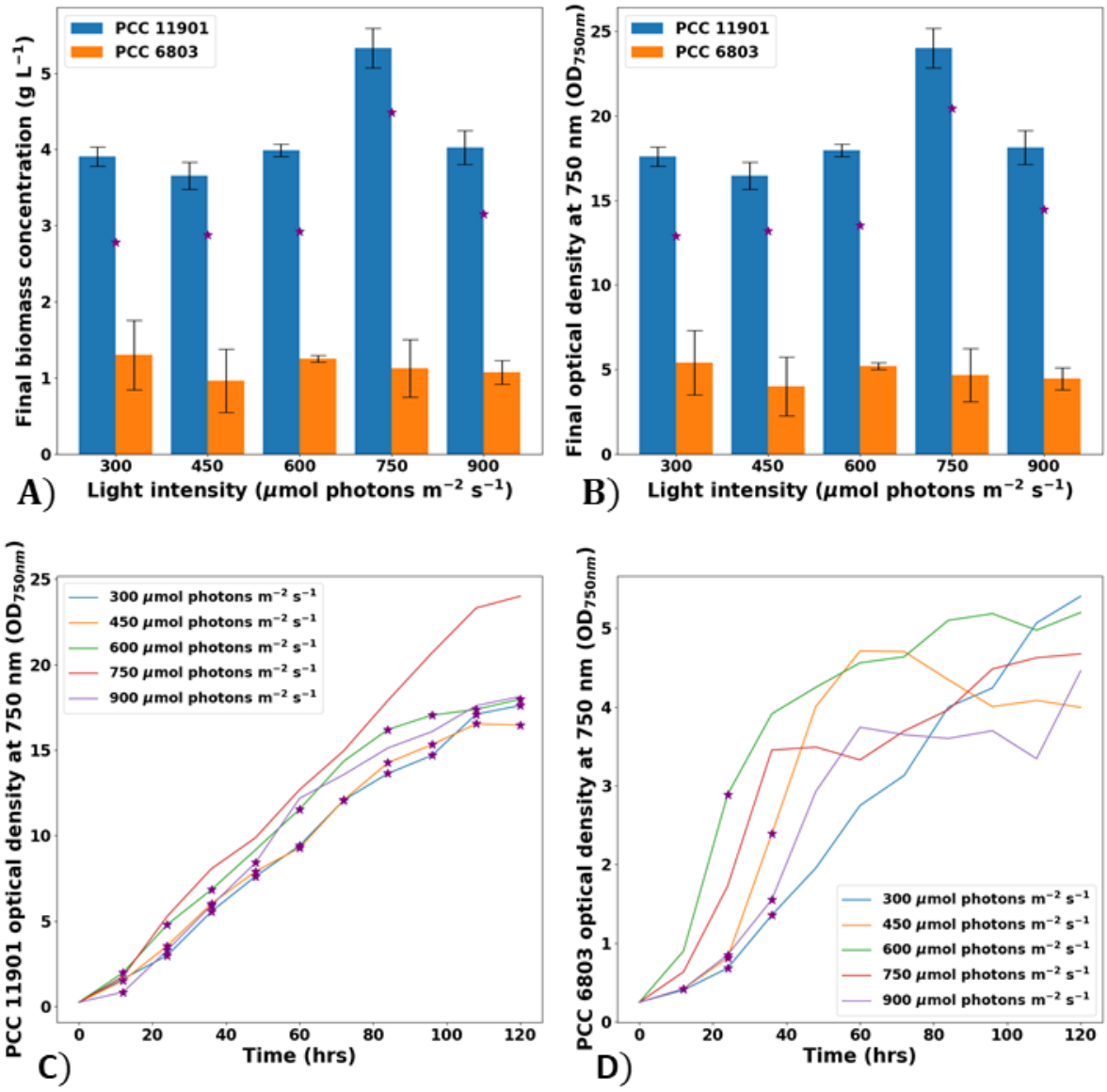

Figure 2: Light intensity influences on biomass production and optical density accumulation in the two cyanobacteria strains. A) final biomass concentration and B) final optical density (OD_{750nm}). Profiles of optical density (OD_{750nm}) for C) PCC 11901 and D) PCC 6803. Purple asterisks indicate significant statistical differences ($P<0.05$) at the various light intensities and time instances: (i) between PCC 11901 and PCC 6803 as presented in A) and B), and (ii) individual growth profiles of PCC 11901 and PCC 6803 as presented in C) and D) respectively. Error bars on plotted data points represent mean of n = 4 biological repeats $\pm$ standard deviation.

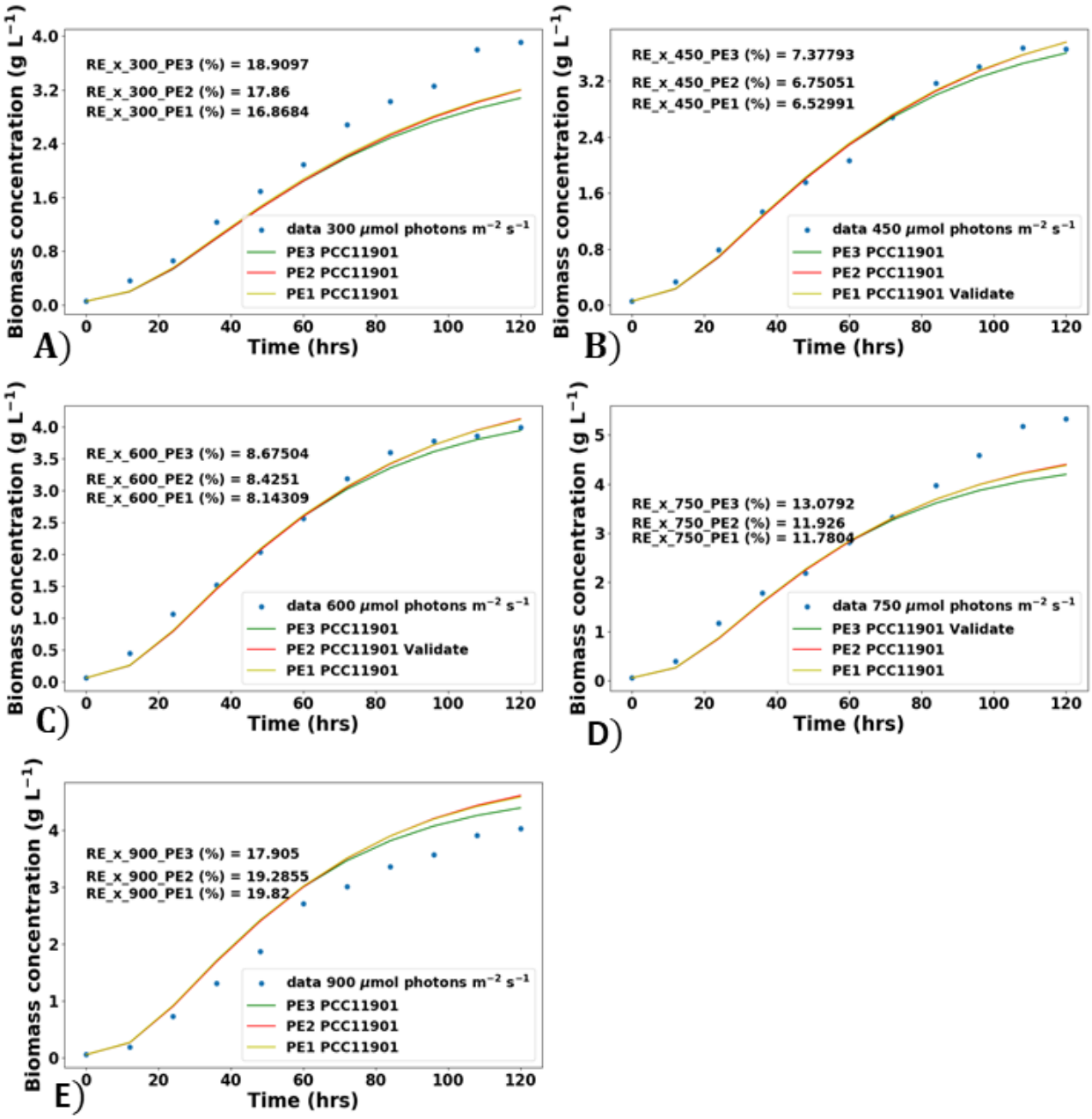

Figure 3: Bootstrapping biomass model fitting results for PCC 11901 at: (A) 300 μmol photons m^{-2} s^{-1}, (B) 450 μmol photons m^{-2} s^{-1}, (C) 600 μmol photons m^{-2} s^{-1}, (D) 750 μmol photons m^{-2} s^{-1}, (E) 900 μmol photons m^{-2} s^{-1}. The percentage relative error (%RE) of each fitting is as indicated.

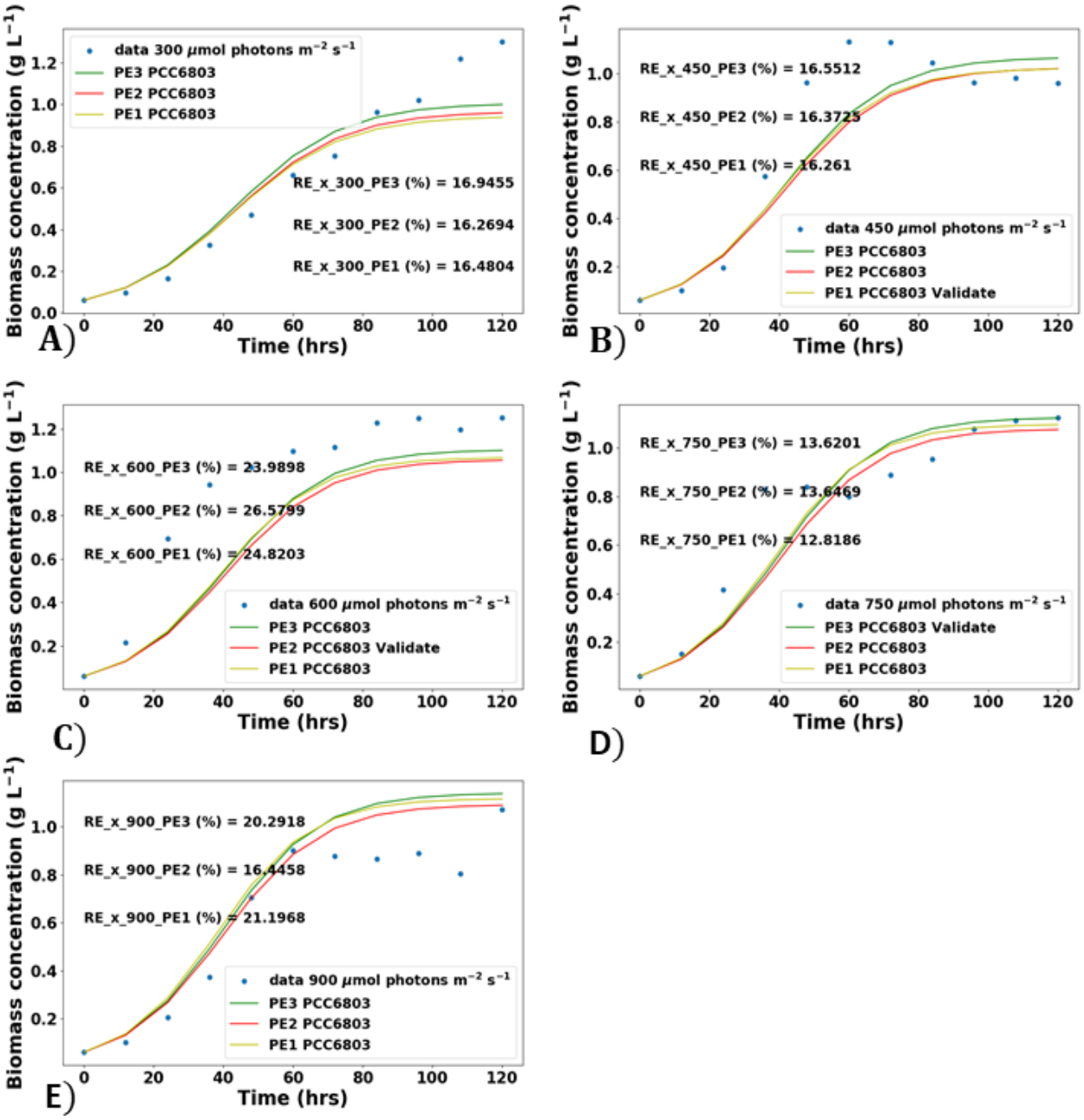

Figure 4: Bootstrapping biomass model fitting results for PCC 6803 at: (A) 300 μmol photons m^{-2} s^{-1}, (B) 450 μmol photons m^{-2} s^{-1}, (C) 600 μmol photons m^{-2} s^{-1}, (D) 750 μmol photons m^{-2} s^{-1}, (E) 900 μmol photons m^{-2} s^{-1}. The percentage relative error (%RE) of each fitting is as indicated.

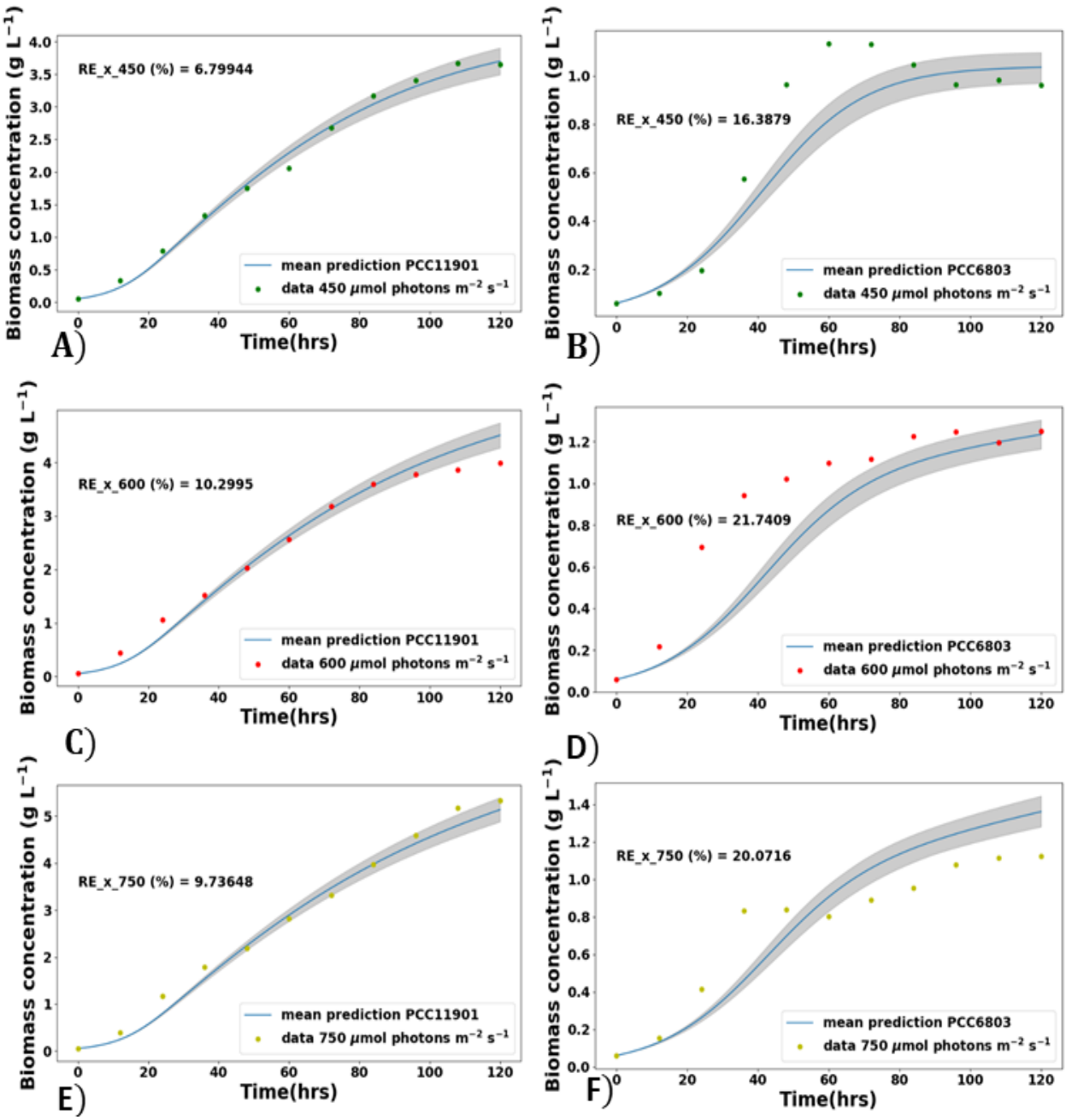

Figure 5: Prediction of biomass models under uncertainty: (A), (C) and (E) for PCC 11901, and (B), (D) and (F) for PCC 6803, at 450, 600 and 750 μmol photons m^{-2} s^{-1}, which were unseen experimental data sets during the bootstrapping parameter estimation. The percentage relative error (%RE) of each fitting is as indicated in grey.

List of Tables

Table 1: Summary of stepping up light intensities used prior to final target light intensity.

Initial PBR light intensity (µmol photons m^{-2} s^{-1})	**PBR step-up light intensity (µmol photons m^{-2} s^{-1})**	**Final PBR light intensity (µmol photons m^{-2} s^{-1})**
150	n/a	300
150	300	450
150	300	600
150	450	750
150	500	900

n/a: not stepped up

Table 2: Bootstrapping design of experiments for model parameter estimation.

Label	**Training data sets (µmol photons m^{-2} s^{-1})**	**Cross validation data sets (µmol photons m^{-2} s^{-1})**
Parameter estimation 1 (PE 1)	300, 900, 600, 750	450
Parameter estimation 2 (PE 2)	300, 900, 450, 750	600
Parameter estimation 3 (PE 3)	300, 900, 450, 600	750

Table 3: Bootstrapping dynamic parameter estimation results for the optical density (OD_{750nm}) and biomass models of the two cyanobacterial strains. Parameter estimates represent the mean of n=3 bootstrapping partitions $\pm$standard deviations as the confidence intervals.

Model parameter	**OD_{750} model**	**Biomass model**	**Literature range**
	PCC 11901		
u_m (h^{-1})	1.99×10^{-1} $\pm 2.86\times10^{-3}$	1.99×10^{-1} $\pm 5.39\times10^{-4}$	(0.004, 0.28)[1–3]
μ_d (h^{-1})	6.15×10^{-4} $\pm 8.94\times10^{-6}$	2.96×10^{-3} $\pm 2.64\times10^{-4}$	(8.559×10^{-3}, 0.005) [3–5]
k_s (µmol photons m^{-2} s^{-1})	150.0 ± 4.08	156.67 ± 6.24	(70.0, 347.0)[1,3,6]
k_i (µmol photons m^{-2} s^{-1})	3523.33 $\pm$ 24.94	3522.33 $\pm$ 23.61	(457.0, 53370)[5,6]
τ (mm^2 g^{-1})	48.57 ± 1.03	208.14 ± 6.62	(67, 225)[3,6]
β (mm^{-1})	na	3.16×10^{-7} $\pm 3.07\times10^{-8}$	0.0[7]
	PCC 6803		
u_m (h^{-1})	7.9×10^{-2} $\pm 2.65\times10^{-3}$	7.9×10^{-2} $\pm 2.65\times10^{-3}$	(0.004, 0.28)[1–3]
μ_d (h^{-1})	1.57×10^{-2} $\pm 3.52\times10^{-4}$	6.54×10^{-2} $\pm 1.46\times10^{-3}$	(8.559×10^{-3}, 0.005) [3–5]
K_s (µmol photons m^{-2} s^{-1})	72.84 ± 12.74	72.84 ± 12.74	(70.0, 347.0)[1,3,6]

na: not included in model structure

Table 4: Analysis of the experimental data sets to determine the magnitude of difference in biomass and optical density accumulation among the two cyanobacterial strains at various light intensities. The scale of ratio corresponds to PCC 11901: PCC 6803.

Species	**Highest observed value at different light intensities (µmol photons m^{-2} s^{-1})**		
	300	750	900
	Biomass concentration (g L^{-1})		
PCC 11901	3.91	5.33	4.02
PCC 6803	1.24	1.37	1.07
Scale of ratio	**3.15**	**3.89**	**3.76**
	OD_{750}		
PCC 11901	17.61	24	18.13
PCC 6803	5.40	5.20	4.46
Scale of ratio	**3.26**	**4.62**	**4.07**

Commented [AB1]: This addresses the comments of reviewer 2 regarding units.

References

[1] Dechatiwongse P, Srisamai S, Maitland G, Hellgardt K. Effects of light and temperature on the photoautotrophic growth and photoinhibition of nitrogen-fixing cyanobacterium Cyanothece sp. ATCC 51142. Algal Res 2014;5:103–11. https://doi.org/10.1016/j.algal.2014.06.004.

[2] Włodarczyk A, Selão TT, Norling B, Nixon PJ. Newly discovered Synechococcus sp. PCC 11901 is a robust cyanobacterial strain for high biomass production. Commun Biol 2020;3. https://doi.org/10.1038/s42003-020-0910-8.

[3] Zhang D, Dechatiwongse P, del Rio-Chanona EA, Maitland GC, Hellgardt K, Vassiliadis VS. Dynamic modelling of high biomass density cultivation and biohydrogen production in different scales of flat plate photobioreactors. Biotechnol Bioeng 2015;112:2429–38. https://doi.org/10.1002/bit.25661.

[4] del Rio-Chanona EA, Dechatiwongse P, Zhang D, Maitland GC, Hellgardt K, Arellano-Garcia H, et al. Optimal Operation Strategy for Biohydrogen Production. Ind Eng Chem Res 2015;54:6334–43. https://doi.org/10.1021/acs.iecr.5b00612.

[5] Cabello J, Morales M, Revah S. Dynamic photosynthetic response of the microalga Scenedesmus obtusiusculus to light intensity perturbations. Chemical Engineering Journal 2014;252:104–11. https://doi.org/10.1016/j.cej.2014.04.073.

[6] Zhang D, Dechatiwongse P, del Rio-Chanona EA, Maitland GC, Hellgardt K, Vassiliadis VS. Modelling of light and temperature influences on cyanobacterial growth and biohydrogen production. Algal Res 2015;9:263–74. https://doi.org/10.1016/j.algal.2015.03.015.

[7] Rio-chanona EA, Ahmed N rashid, Zhang D, Lu Y, Jing K. Kinetic Modeling and Process Analysis for Desmodesmus sp. Lutein Photo-Production. AICHE Journal 2017;63:2546–54. https://doi.org/10.1002/aic.

Declaration of interests

☒The authors declare that they have no known competing financial interests or personal relationships that could have appeared to influence the work reported in this paper.

☐The authors declare the following financial interests/personal relationships which may be considered as potential competing interests:

Authors statement

Bovinille Anye Cho's contributions included construction of the mechanistic model, proposing design of experiments, analysing generated data and results, and drafting of the manuscript. José Ángel Moreno-Cabezuelo and Lauren A. Mills performed the *Synechococcus* sp. PCC 11901 and *Synechocystis* sp. PCC 6803 cultivation experiments, drafting of the manuscript, and manuscript revision. Ehecatl Antonio del Río Chanona and Dongda Zhang supervised the mechanistic modelling, optimisation, design of experiments, and provided valuable insights for important intellectual content. David J. Lea-Smith supervised the cultivation experiments, and critically revised the manuscript for important intellectual content. Dongda Zhang and David J. Lea-Smith gave the final approval of the article.

Integrated experimental and photo-mechanistic modelling of biomass and optical density production of fast versus slow growing model cyanobacteria

Commented [AB1]: This addresses the comment of reviewer 1 regarding title change.

Bovinille Anye Cho[1,*], José Ángel Moreno-Cabezuelo[2], Lauren A. Mills[2], Ehecatl Antonio del Río Chanona[3], David J. Lea-Smith[2], Dongda Zhang[1]

1. School of Engineering, Department of Chemical Engineering, University of Manchester, Engineering Building A, Oxford Road, Manchester, M13 9PL, UK.
2. School of Biological Sciences, University of East Anglia, Norwich Research Park, Norwich, NR4 7TJ, United Kingdom
3. Department of Chemical Engineering, Imperial College London, South Kensington Campus, London SW7 2AZ, UK.

*: Corresponding author, Bovinille Anye Cho: email: bovinille.anyecho@manchester.ac.uk, tel: 44 (0) 744 848 5377.

Abstract

Biotechnological exploitation of fast-growing cyanobacterial species is hindered by unavailable mechanistic interpretations for the differing bioconversion rates when exploring strains with similar metabolic pathways and transport systems. This study investigated two strains: *Synechococcus* sp. PCC 11901, the fastest growing cyanobacterium identified to date, and *Synechocystis* sp. PCC 6803, under a range of operational light intensities from 300 - 900 µmol photons m^{-2} s^{-1}, and presents three original contributions. Firstly, strain specific dynamic biomass and optical density (OD_{750nm}) models were constructed incorporating sophisticated photo-mechanistic influences, previously unachieved in OD_{750nm}. Secondly, bootstrapping parameter estimation with 3-fold cross validations was exploited to simultaneously identify the model parameters and confidence intervals, thus enabling probabilistic simulations and thorough validation against experimental data sets. Thirdly, presented mechanistic interpretations for the over two-fold faster growth of PCC 11901 versus PCC 6803 despite PCC 6803's high light utilisation efficiency. These findings will benefit upscaling of future cyanobacterial biotechnology applications and exploitation of *Synechococcus* sp. PCC 11901 for production of biomass and chemicals of industrial, nutritional and medical importance.

Keywords: Cyanobacterial biotechnology; *Synechococcus* sp. PCC 11901; *Synechocystis* sp. PCC 6803; Light attenuation; Biomass and OD dynamic modelling.

1. Introduction

Cyanobacteria are potential chassis for converting inorganic carbon into biomass and biomolecules for industrial (e.g., isoprene [1]), nutritional (e.g., glucose/fructose mixture [2]), medical (e.g., mycosporine and mycosporine-like amino acids [3]), and herbicidal (e.g., antimetabolite 7-deoxy-sedoheptulose [4]) applications. Utilising light, minimal nutrients and potentially low-cost waste streams like flue gases (e.g., 4-14 vol% CO_2 from power plants [5–7]), with facilities not requiring arable land, cyanobacterial production of biomolecules could be industrially attractive for carbon capture and the sustainable production of biorenewable compounds. However, to improve commerciality, overall cyanobacterial productivity (i.e., amount of product per time) and product titer (i.e., amount of product per volume) needs to be comparable to alternative industrially viable heterotrophic microorganisms like *Escherichia coli* and *Saccharomyces cerevisiae* with doubling times of 20 and 90 minutes, respectively [8].

For this reason, significant research efforts has been invested in isolating cyanobacterial species that grow faster than the most commonly studied and genetically tractable model organisms such as *Synechocystis* sp. PCC 6803 (PCC 6803) [8–10] and *Synechococcus elongatus* PCC 7942 (PCC 7942) [9,10] with doubling times of 6.6 and 4.1 hours, respectively [8]. *Synechococcus* sp. PCC 7002 (PCC 7002) [9–11] and more recently, *Synechococcus elongatus* UTEX 2973 (UTEX 2973) [9–12], and *Synechococcus* sp. PCC 11901 (PCC 11901) [8,10] with respective doubling times of 4.0 hours [8,9], 2.1 hours [9] and 2.0 hours [10], have been partially characterised. A comparison of these species showed that PCC 11901 demonstrated the fastest growth and highest biomass accumulation (up to 33 g DCW L^{-1} [10]), suggesting it is the most promising species for future biotechnology applications. Faster growth may be due to a range of factors but could be linked to lower photoinhibition, higher photosynthetic rates, and higher light utilisation efficiency in PCC 11901 than other model species [8]. Surprisingly, PCC 11901 and PCC 6803 were shown to have very similar metabolic pathways and transport

systems [8]. Despite these similarities, in-depth mechanistic analysis via estimated biokinetic model parameters, which could provide additional physical, chemical, biological and interacting explanations for the observed growth capabilities, have not been conducted. Previous studies either (i) directly compared the obtained final biomass concentrations and/or optical densities [10,13], and/or (ii) experimentally measured the oxygen evolution and photoinhibition rates [8], and/or (iii) curve fit for the maximum specific growth rate with the experimentally generated data of biomass concentrations and/or optical densities [10,12]. As a result, doubling times are grossly estimated without accounting for the impact of process equipment (e.g., photobioreactor path length), operation (e.g., light intensity and light attenuation), and growth dynamics (e.g., photolimitation, photosaturation and photoinhibition). This makes it challenging to compare PCC 11901 to industrially viable heterotrophic microorganisms with reported doubling times from scalable bioreactor layouts (i.e., lab to the industrial scale). For example, investigations of PCC 11901 have been so far limited to <100 mL PBRs [8] but directly compared to *Saccharomyces cerevisiae* investigations from a 1 L fermenter [14].

Combining experimental observations with dynamic mechanistic approaches has been exploited in previous studies. For example, Clark *et al*., [11] exploited dynamic models to compare light-limited cyanobacterial growth of PCC 7002 and UTEX 2973 in differing experimental systems by comparing their photosynthetic efficiencies. Unlike Clark *et al*., [11] whereby the growth dynamics were limited to the stationary growth phase, all other cyanobacterial growth phases (i.e., primary, secondary, and stationary) except the lag phase were comprehensively described mechanistically by Zhang *et al*., [15] and Del Rio-Chanona, *et al*., [16] for *Cyanothece* sp. ATCC 51142. Dechatiwongse *et al*., [17] implemented two dynamic models: a logistic model for optical density and an inverse logistic model for nutrient uptake, in describing the effects of light intensity and photoinhibition on *Cyanothece* sp. ATCC

51142. Although they investigated a wide range of light intensities (i.e., 23 to 320 µmol photons m^{-2} s^{-1}) in a 3L tubular Photobioreactor (PBR), the influence of light attenuation was not accounted for within their dynamic models.

Accounting for light attenuation is of utmost importance when analysing fast growing strains. In dense cultures, cells in the front-facing PBR section will harvest the majority of light, leading to higher levels of photoinhibition [18,19]. Cells in the interior will receive less light and may become photolimited, consequentially affecting the overall reported growth rate of the culture. These growth dynamics have been successfully modelled using the Beer-Lambert Law and Aiba model for light attenuation and photomechanisms (i.e., photolimitation, photosaturation and photoinhibition), respectively, in the literature [20–23]. However, these studies were mainly focused on the construction of dynamic biomass production models and the incorporation of light attenuation and photomechanisms into dynamic optical density models has not been performed.

To address these limitations we aim to embed the impact of light intensity, light attenuation, photolimitation, photosaturation and photoinhibition photomechanisms in assessment of growth via biomass accumulation and OD_{750nm} measurements, and scalability potential of two cyanobacterial species: PCC 11901 and PCC 6803. Specifically, we will: (i) analyse differences in biomass accumulation and growth via optical density measurements within a wide range of environmentally relevant light intensities from 300 to 900 µmol photons m^{-2} s^{-1}, (ii) construct dynamic predictive models for biomass production and optical density measurements, unifying the complicated influences of incident light intensity, light attenuation and photomechanisms to support the explanations of experimental results via comparison of the estimated biokinetic model parameters, and (iii) provide in-depth mechanistic discussion and identification of the optimal light intensities for cultivation and biotechnological scalabilities of the strains.

2. Materials and modelling methods

2.1 Bacterial species, media, and starter culture growth conditions

Two cyanobacterial species, PCC 11901 (a kind gift from Peter Nixon, Imperial College London) and PCC 6803 [24] were maintained on AD7 and BG11 agar plates, respectively, as previously described in [13] and [10]. Cells scraped off plates were used to seed starter cultures grown in their corresponding liquid medium of 50 mL in 100 mL conical flasks. Conical flasks were shaken at 120 rpm while being maintained at a temperature of 30 °C and under a light intensity of 40 µmol photons m^{-2} s^{-1} as provided by a warm white LED light in an Algaetron 230 growth chamber (Photon Systems Instruments, Czech Republic).

2.2 Photobioreactor setup and operation

Strains were cultured in 100 mL cultivation tubes in a MC-1000 multicultivator bioreactor equipped with a warm white LED light source having a radiating capacity up to 1000 µmol photons m^{-2} s^{-1} (Photon Systems Instruments, Czech Republic) (see Fig. 1). Each cultivation tube had an external and internal diameter of 30 mm and 27 mm, respectively. Cells were sparged with air/5% CO_2 to supplement the supply of inorganic carbon and mix the cells; this was maintained at a temperature of 38 °C. Optical density was quantified using a Jenway 6305 Genova UV/VIS (Genova, United Kingdom) spectrophotometer set at a wavelength of 750 nm. Initially, the PBR was illuminated at 150 µmol photons m^{-2} s^{-1} and 80 mL of its volume was inoculated with a starter culture of $\mathrm{OD}_{750\mathrm{nm}} = \sim 0.1$, before being incubated for 24 hours. Afterwards, the growing culture was diluted down to $\mathrm{OD}_{750\mathrm{nm}} = \sim 0.1$ and re-inoculated into the PBR for a stepped-up illuminating light intensity (Table 1) for another 24 hour period. Thereafter, the illuminating light intensity was further increased to the final target light intensity (Table 1) and the growing cultures were incubated overnight to adapt to the new PBR conditions. From this culture, samples were removed and diluted to $\mathrm{OD}_{750\mathrm{nm}} = 0.25$, before

starting the growth experiments at the various investigated light intensities (300, 450, 600, 750 and 900 µmol photons m^{-2} s^{-1}). Growth experiments lasted for 120 hours and 1 mL samples were removed for analysis from the PBR at 12 hours interval during this cultivation time.

2.3 Analytical methods

The state variables of interest herein were the (i) optical density measured at a wavelength of 750 nm (OD_{750nm}) and (ii) cell dry weight, X (g L^{-1}) (referred to as biomass concentration thereafter). Biomass concentration was determined from established standard curves between X and OD_{750nm} as reported in Eq. (1) and (2) for PCC 11901 and PCC 6803 respectively. These standard curves were achieved by harvesting densely grown cultures from the PBR after 120 hours. Cells were centrifuged at 5,000 x g with a Centrifuge 5804 R (Eppendorf, Germany) and washed twice with sterile deionised water. The samples were diluted to 10%, 20%, 40%, 60%, 80% and 100%, recorded for OD_{750nm} at each serial dilution, with 5 mL of the serial dilution aliquoted on a pre-weighed filter paper of 70 mm diameter (i.e., Whatman GF/B Glass Microfibre Filters, USA). Prior to this, the filter paper had been dried for 48 hours at 70°C in an oven (Binder BD-S 056, Germany) and then weighed with a microbalance (Kern ABT 220-SDNM, Germany). Cells on the dried filter paper were left at 24 hours at 70°C, then weighed in triplicate.

Commented [AB2]: This addresses the comment of reviewer 2 regarding typo.

$$X_{\mathrm{PCC\_11901}}(\mathrm{g\ L^{-1}}) = 0.222 \cdot OD_{750nm\_\mathrm{PCC\_11901}}\,, \quad \mathrm{R}^2 = 0.998 \tag{1}$$

$$X_{\mathrm{PCC\_6803}}(\mathrm{g\ L^{-1}}) = 0.2406 \cdot OD_{750nm\_\mathrm{PCC\_6803}}\,, \quad \mathrm{R}^2 = 0.996 \tag{2}$$

2.4 Mathematical model construction

The constructed dynamic models were used to simulate state variables under the sophisticated influences of (i) incident light intensity, (ii) light attenuation, and (iii) photomechanisms.

However, the differing magnitude of light related influences among the two investigated cyanobacterial strains implied their experimental data sets would first need to be subjected to statistical student *t*- test(s) to inform the incorporation of either all (i.e., (i), (ii) and (iii)) or a selective combination (e.g., (i) and (iii) only) of these light related influences.

2.4.1 Modelling of biomass concentrations

The two cyanobacterial species were expected to exhibit the four different growth phases (namely the (i) lag phase, (ii) primary growth phase (iii) secondary growth phase, and (iv) stationary phase), as reported in other studies [15–17]. Herein, the lag phase was not pronounced due to the starter cultures being adapted to the operational light intensity of the PBR by using the light stepping up strategy as reported in Table 1. Therefore, the dynamic model structure in Eq. (3) was constructed to capture the three remaining phases. This model structure permits the incorporation of the strain dependent biological knowledge influencing the trajectories of the state variables. For instance, the light related influences of differing magnitude among the cyanobacterial strains are linked to the growth associated terms (i.e., first term on right hand side of Eq. (3)). Meanwhile, the decay associated terms (i.e., second term on right hand side of Eq. (3)) are often controlled by endogenous cellular respiration activities, thus taking place under dark circumstances, and can be modelled as independent of light.

$$\frac{dX}{dt} = u\,(I) \cdot X - \mu_d \cdot X^2 \tag{3}$$

Where X is the biomass concentration (g L^{-1}), $u\,(I)$ represents the effects of the PBR's light intensities on the biomass growth (h^{-1}) and $\mu_d(I)$ denotes the specific cell decay rate (L g^{-1} h^{-1}).

2.4.2 Modelling of optical densities

Although often disputed as to whether there exist a linear or a non-linear correlation between the biomass concentration and optical density, the optical density profiles of *Synechococcus* and *Synechocystis* strains has been shown [8,10,17] to have sigmoidal shapes. This sigmoidal shape is typical of bioprocesses experiencing the three remainder phases as highlighted in Section 2.4.1. Thus, the model structure of the optical density and biomass concentration (i.e., Eq. (3)) were assumed to be similar. Hence, Eq. (4) was constructed to simulate the optical density profiles of the two cyanobacterial species.

$$\frac{d\ \mathrm{OD}_{750}}{dt} = u\ (I) \cdot\ \mathrm{OD}_{750} - \mu_d \cdot\ \mathrm{OD}_{750}{}^{2} \tag{4}$$

Where OD_{750} is the optical density at a wavelength of 750 nm (dimensionless), $u\ (I)$ represents the effects of the PBR's light intensities on the optical density build up (h^{-1}) and μ_d denotes the specific rate of vanishing optical density (h^{-1}).

2.4.3 Modelling of light intensity, light attenuation, and photomechanisms

Generally, in the literature [15,19,20,23], the effect of light on growth rates are often characterised mechanistically by three distinguishable photomechanisms, namely (i) photolimitation, (ii) photosaturation and (iii) photoinhibition, via the Aiba model structure (Eq. (5)). The former, second and latter occur under low, optimal, and high light intensities, respectively. Under low light intensities, the growth rate increases linearly with increasing light intensity till saturation at the optimal light intensity. Beyond this, the growth rate decreases with further increase in the light intensity. Considering the wide range of investigated light intensities (300 – 900 µmol photons m^{-2} s^{-1}), it was necessary to implement a model that captures all three photomechanisms on the growth associated terms (i.e., first term on right hand side) of Eq. (3) and Eq. (4). However, student *t*- test(s) were first performed on the experimental data sets for statistical significance to confirm the validity of the light influences on the two cyanobacterial strains.

Commented [AB3]: This addresses the comments of reviewer 2 regarding additional details of the Aiba model.

$$u\,(I) = u_m \cdot \frac{I(z)}{I(z) + k_s + \frac{I(z)^2}{k_i}} \tag{5}$$

Where u_m is the maximum specific growth rate (h^{-1}), $I(z)$ denotes the light attenuation model (see Eqs. (6) and (7) below), k_s and k_i are the light saturation (µmol photons m^{-2} s^{-1}) and light inhibition (µmol photons m^{-2} s^{-1}) coefficients respectively.

2.4.3.1 Modelling PCC 11901 growth associated terms

From the student's *t*-test performed over the wide operational light intensity range (300 to 900 µmol photons m^{-2} s^{-1}), statistical significance ($P<0.05$ being statistically significant) of light intensity influences were observed in the data sets of PCC 11901 as further discussed in Section 3.1. Hence, Eq. (5) was employed to encompass all the above mentioned photomechanisms on the associated growth terms (i.e., first term on right hand side of Eq. (3) and Eq. (4)). Eq. (5)'s light attenuation model, based on the unidirectional illumination of the PBR in Fig. 1, was defined by Eq. (6) for the biomass production model (Eq. (3)), and Eq. (7) for the optical density model ((Eq. (4)). Light scattering phenomena is often reported to be significant in the presence of dense cell mass [25,26]. To overcome this, the embedded light attenuation model within the biomass model (Eq. (3)) included both the light absorption and light scattering terms. Only pigment dominated light absorption influences were therefore accounted for within the optical density model. These assumptions were concluded to be rational for a PBR of this size with a short light path length and low aeration rate (no visible gas bubbles during cultivation experiments). We therefore assumed light scattering induced by insignificant gas bubbles to be negligible in the models, especially for the optical density model.

$$I(z) = I_0 \cdot \exp[-(\tau \cdot X + \beta\,) \cdot z] \tag{6}$$

$$I(z) = I_0 \cdot \exp[-(\tau \cdot \mathrm{OD}_{750}) \cdot z] \tag{7}$$

Where I_0 is the operational incident light intensity (µmol photons m^{-2} s^{-1}), z is the light path length (mm) and β is the light scattering coefficient (mm^{-1}). τ is the light attenuation coefficient with units of (mm^2 g^{-1}) and (mm^{-1}) for Eq. (6) and Eq. (7) respectively.

The simplified light attenuation model structures (i.e., Eq. (6) and Eq. (7)) have been reported by Anye Cho *et al*., [27] to be numerically stable for dynamic parameter estimation solvers without compromising the high solution accuracy, as compared to other literature complex light transmission models such as the two-flux approximation of the full radiation transfer equation [25,26]. However, incorporation of the PBR's cylindrical curvature effects in Eq. (6) and Eq. (7) will further increase the model complexity and computational burden for the dynamic parameter estimation solver. Therefore, further simplifications by approximating the observed circular cross-section with a rectangular cross-sectional area as reported in [27,28], and altering the light path length to 23.9 mm, was implemented.

When embedding Eq. (5), Eq. (6), Eq. (7) into Eq. (3) and Eq. (4), the overall predictive model is now a partial differential equation (PDE) due to the presence of both temporal and spatial dimensions, thus challenging to resolve both dimensions for the non-linear optimisation solver. To utilise a less complex ordinary differential equation (ODE) solver, a 20-step trapezoidal rule, as shown in Eq. (8), was employed to eliminate the spatial dimensions [15,19] in the model. Opposed to the commonly utilised 10-step trapezoidal rule in the literature [15,16,19], the extra number of trapezoidal steps were motivated by the observed higher magnitudes of biomass concentration (~ 5.3 g L^{-1} herein) and optical density (~ 24 herein) in PCC 11901 over that in the literature (< 3 g L^{-1}) [15,16] for slower growing cyanobacterial species. Therefore, the predictive models of PCC 11901 required more integration steps to better approximate its spatial dimension related parameters (i.e., u_m, k_s and k_i) during the parameter estimation process. Hence, Eqs. (6), (7), and (8) were then substituted into Eqs. (3) and (4) for the remainder of this study.

$$u\,(I) = \frac{u_m}{40} \cdot \sum_{n=1}^{19} \left(\frac{I_0}{I_0 + k_s + \frac{I_0^2}{k_i}} + \frac{2 \cdot I_{\frac{n \cdot L}{20}}}{I_{\frac{n \cdot L}{20}} + k_s + \frac{I_{\frac{n \cdot L}{20}}^2}{k_i}} + \frac{I_L}{I_L + k_s + \frac{I_L^2}{k_i}} \right) \tag{8}$$

2.4.3.2 Modelling PCC 6803 growth associated terms

Contrary to the statistically significant difference in PCC 11901, the final biomass and optical density datasets of PCC 6083 showed statistical insignificance (P>0.05) over the light intensity range (300 - 900 µmol photons m^{-2} s^{-1}) and was therefore not experiencing the above mentioned photomechanisms. However, upon performing dynamic student's *t*-test(s) over each state trajectory as discussed in Section 3.1, two to three discrete time points on each growth trajectory did show some level of statistical significance as seen in Fig. 2D, thereby implying a partial presence of these photomechanisms. Since these points were observed mostly around the exponential growth phase (i.e., between 20 and 60 hours), light saturation to a smaller extent was assumed present. Meanwhile, photoinhibition was completely ruled out (i.e., $\left[\frac{I(z)^2}{k_i}\right] \sim 0$ in Eq. (5)) as growth of PCC 6083 was not observed to decline over time and operational light intensities. However, the very small extent of light saturation implied that the influence of light attenuation on growth of PCC 6083 was also negligible (i.e., $\tau = \beta = 0$ in Eqs. (6) and (7)), thereby leading to Eq. (9). This resulting Monod-like model structure theoretically implies that the growth of PCC 6083 will increase linearly at lower operational light intensity until a saturation threshold is attained whereby the growth becomes maximal and independent of the operational light intensity. Herein, the former linear increase was assumed to only occur below 300 µmol photons m^{-2} s^{-1}, and the proposed model was therefore valid to simulate the saturating threshold (300 - 900 µmol photons m^{-2} s^{-1}) when embedding Eq. (9) into Eq. (3) and (4).

$$u\,(I) = u_m \cdot \frac{I_0}{I_0 + K_s} \tag{9}$$

Where K_s represent the light saturation (µmol photons m^{-2} s^{-1}).

2.5 Model parameter estimation methodology

To estimate the model parameters, a weighted non-linear least-square regression problem (see Eqs. (10a) to (10e)) was formulated. Due to the stiffness and high non-linearity of the proposed biomass and optical density models, orthogonal collocation over finite elements in time was utilised to numerically discretise the differential equations, thus transforming them into a series of non-linear algebraic equations. Thereafter, the resulting non-linear optimisation problem was solved with an interior point-based solver (i.e., IPOPT [29] version 3.11.1) through an open-source interface Pyomo [30,31] within the Python version 3.9 programming environment.

$$\min_{P} \Phi(\boldsymbol{p}) = \sum_{k=1}^{Nspp} \sum_{j=1}^{NV} \sum_{i=1}^{NP} \left(\frac{\hat{y}_{i,j,k} - y_{j,k}(t_i, \boldsymbol{p})}{\hat{y}_{i,j,k}} \right)^{\mathbf{2}} \cdot w_{i,j,k} \tag{10a}$$

Subject to:

$$\frac{d\boldsymbol{y}}{dt} = f(\boldsymbol{y}(t), p)\,, \qquad t \in [t_0, t_f] \tag{10b}$$

$$\boldsymbol{y_{lb}} \leq \boldsymbol{y} \leq \boldsymbol{y_{ub}} \tag{10c}$$

$$\boldsymbol{p_{lb}} \leq \boldsymbol{p} \leq \boldsymbol{p_{ub}} \tag{10d}$$

$$\boldsymbol{y}(t_0) = \boldsymbol{y_0} \tag{10e}$$

whereby $\boldsymbol{p}$ denotes a vector of parameters, $Nspp$, NV and NP are the number of species (i.e., PCC 11901 and PCC 6803), number of state variables (i.e. biomass concentration and optical density) and number of experimental data points, respectively, $\boldsymbol{y}$ denotes dynamic model output, $\hat{y}_{i,j,k}$ represents the experimental data point of species k with state variable j at time instant t_i, w_i is a weighting factor of species k for the data point of state variable j at time instant t_i, $\boldsymbol{y_{lb}}$, $\boldsymbol{y_{lb}}$, $\boldsymbol{p_{lb}}$ and $\boldsymbol{p_{ub}}$ denotes the lower and upper bounds of the state variables and

parameters, respectively, t_0 and t_f represents the initial and final cultivation times, $\boldsymbol{y_0}$ denotes the initial concentration of the state variables.

To simultaneously identify all model parameters as well as their confidence intervals, a bootstrapping technique was applied. This has increasingly been used in the machine learning community [32–34] for quantification of uncertainties. By implementing the bootstrapping methodology, the entire experimental dataset (i.e., 300 - 900 µmol photons m^{-2} s^{-1}) were repartitioned into PE1, PE2 and PE3 as illustrated in Table 2. Eqs. (10a) to (10e) were solved on every partition for dynamic model parameter estimation. The obtained parameter estimates were statistically aggregated by averaging for the mean and standard deviation. As a caveat, the upper and lower bounds of the experimental data sets (i.e., 300 and 900 µmol photons m^{-2} s^{-1}) were included in all three data partitions (Table 2). This was to guarantee the models high-fidelity extrapolations within the investigated range. This was later confirmed with a separate cross validation data set which was not utilised during parameter estimation (Table 2).

To evaluate the impact of the parameter confidence intervals on the various model prediction uncertainties, a Latin Hypercube Sampling methodology was used to draw 100 probabilistic samples from the confidence intervals. For each probabilistic sample, a dynamic model simulation was performed thereby amounting to a total of 100 Monte Carlo simulations whereby the mean prediction was computed and compared against the unseen experimental data sets. This implementation was carried out in Python version 3.9 using the *SMT* 1.0.0 and *Numpy* libraries.

3. Results and discussion

3.1 Evaluating the influence of light intensity on cyanobacterial growth

Cultures of PCC 11901 and PCC 6803 were grown at five different light intensities (300, 450, 600, 750 and 900 µmol photons m^{-2} s^{-1}), in order to investigate their growth dynamics over a wide range covering the low, medium, and high light intensities responsible for

photolimitation, photosaturation and photoinhibition respectively. Since the initial biomass concentrations and optical densities upon inoculation of the PBR were the same for all five investigated incident light intensities, the obtained final biomass concentrations and OD_{750nm} after 120 hrs of photoautotrophic growth were firstly analysed with student's *t*-test ($P<0.05$ being statistically significant) to identify the experimental light intensity (i.e., I_{0_opt}) that resulted in the highest biomass and OD_{750nm}. Thereafter, the entire biomass and OD_{750nm} time evolution profiles corresponding to I_{0_opt} were analysed with the remaining four data sets via a student's *t*-test ($P<0.05$ being statistically significant) for the effects of incident light intensity on the individual cyanobacterial strains.

The highest accumulation of biomass concentration and OD_{750nm} in PCC 11901 was observed at 750 µmol photons m^{-2} s^{-1} with corresponding values of 5.33 g DCW L^{-1} and OD_{750nm} = 24 (Fig. 2; Table 4). Biomass accumulation was similar between 300 to 600 µmol photons m^{-2} s^{-1}. From 750 to 900 µmol photons m^{-2} s^{-1}, biomass accumulation decreased by 24.6 % to 4.02 g DCW L^{-1}. A similar trend was observed in the OD_{750nm} measurements. The increase from 300/450/600 to 750 µmol photons m^{-2} s^{-1} suggests that cultivation of PCC 11901 below 750 µmol photons m^{-2} s^{-1} is suboptimal, possibly resulting in lower photosynthetic electron transport rates not sufficient for optimal carbon fixation [35].

Conversely, the decrease from 750 to 900 µmol photons m^{-2} s^{-1} could be due to photoinhibition [35], thus reducing the electron transport rate. It therefore confirms the use of Eq. (5) in Section 2.4.3 to mechanistically describe the three distinguishable photomechanisms, namely (i) photolimitation, (ii) photosaturation and (iii) photoinhibition. This further validates the implementation of the dynamic modelling approach to account for the dynamic light intensity effects on growth of PCC 11901. Fig. 2C shows the existence of statistical significance ($P<0.05$) over the entire trajectory and not just the final biomass concentration and OD_{750nm} in Fig. 2A.

The final biomass concentration and OD_{750nm} of PCC 6803 showed no statistically significant difference ($P > 0.05$) over the 300 to 900 µmol photons m^{-2} s^{-1} range (Fig. 2B). This was unexpected and could be due to the light intensity saturation threshold of PCC 6803 being lower than 300 µmol photons m^{-2} s^{-1}, which is when cultivation of PCC 6803 is typically performed [9]. However, the lack of declining growth due to photoinhibition within this 300 to 900 µmol photons m^{-2} s^{-1} range could be due to the light adaptation strategy outlined in Table 2. This may allow cells to acclimate to constant quantum yields, thus engendering similar rates of electron transport, even at the higher light intensities, and thus already at the theoretical maximum production rates of biomass and OD_{750nm} (Fig. 2B). However, it should be noted that this has not been observed in other studies [8–10], thus further experiments (e.g., fluorometry measurements [35,36]) to quantify electron transport should be conducted. This data could also be used to perform a Dynamic Flux Balance Analysis (DFBA) [37] which could lead to strategies for engineering the light absorption and light utilisation mechanisms of PCC 6803 in order to optimise this species for higher light intensities (i.e., >300 µmol photons m^{-2} s^{-1}) to achieve maximum titer and yields.

3.2 Mathematical model-based analysis

Commented [AB4]: This addresses the comments of reviewer 2 regarding rephrasing the title.

3.2.1 Parameter estimation results

For the constructed dynamic models to yield reliable predictions of the observed biomass and optical density state variables, all model parameters must first be identified in a precise and accurate manner. Second, the estimated model parameters have associated uncertainties which, if known, can aid the model's predictions, allowing fidelities to be assessed and enabling the implementation for bioprocess control and optimisation. The bootstrapping technique is often utilised for this uncertainty quantification in machine learning models [32,33,38] and was herein adapted for this analysis, as discussed in Section 2.5. Table 3 lists the identified mean

parameter values for *n*=3 bootstrapping partitions and their standard deviations for both the optical density and biomass models respectively. These parameter results were compared against those available from previous studies as seen in the last column of Table 3, showing that they were well within the range from previous studies [10,16,17,22,23,39]. The sole exception was for the OD light absorption coefficient which was previously unavailable and therefore compared against those from previous literature biomass models [22,23], which generally agreed with our outcomes and thereby validated the reliability of the presented results.

Figure 3 and 4 show the predicted biomass model fit against the experimental data points from which the optimal parameter results in Table 3 were obtained via the bootstrapping technique. The fittings of the biomass and $\mathrm{OD}_{750\mathrm{nm}}$ models were similar as justified by their equally obtained percentage relative errors (%RE) (i.e., circa 13.8 % and 18.0 % for PCC 11901 and PCC 6803). Therefore, only the biomass model fittings were shown herein while the $\mathrm{OD}_{750\mathrm{nm}}$ model fittings were presented in Figs. S1 and S2. An in depth analysis of the model fitting results were carried out by computing the overall average percentage relative errors (%RE), which showed the model predictions of PCC 11901 (i.e., 13.8 %) to follow the experimental datasets better than the one of PCC 6803 (i.e., 18.0 %), with similar observations for the cross validation runs (i.e., 9.3% and 18.8 % respectively). Whilst this was expected due to the larger standard deviation between the experimental datasets observed in PCC 6803 (Fig. 4 and Fig. S2), it was deemed acceptable when considering that typical light driven bioprocesses are often associated with larger uncertainties [27,40]. Nonetheless, all the model trajectories were seen to represent the experimental data points, thereby capturing the underlying complex behaviours with a small subset of biokinetic parameters. This confirms that the postulated mechanistic hypothesis during the model construction and implemented model structural simplifications for the dynamic parameter estimation solver were all valid.

3.2.2 Probabilistic model predictive validations

To utilise the constructed dynamic models for estimating the optimal operating conditions for industrial use of strains, as well as for model implementation during long-term bioprocess simulation, optimisation and control, it was necessary to evaluate the model performances for predicting unseen experimental data sets. Since the experimental data sets at 450, 600 and 750 μmol photons m^{-2} s^{-1} represented the cross validation runs in Table 2 and without embedded uncertainties, the same conditions were simulated upon embedding the aggregated bootstrapping uncertainties. For this, 100 Monte Carlo simulations were performed by sampling the model parameter confidence intervals in Table 3 and propagating their influences on the dynamic model's output. Fig. 5 shows the biomass model predictions under uncertainty for the two cyanobacterial strains. The mean prediction from the uncertainty bands (in grey) were computed to compare against the experimental data points. Whilst the uncertainty bands reflect the degree of variability imposed by the parameter confidence intervals, those for the biomass and optical density models were similar. Thus, only those for the biomass model were shown in Fig. 5 while those of the optical density models are presented in Fig. S3. These uncertainty bands are observed to grow (i.e., increase of bandwidth size) with time, indicating the models to be responsive to changes of these parameters. Generally, as the parameter changes did not induce large uncertainty bands, they are therefore safe for re-estimation during online dynamic bioprocess control. To evaluate the model's prediction under uncertainty versus the pure model outputs, the overall %RE in Fig. 5 were computed (i.e., 8.9 % and 19.4 % for PCC 11901 and PCC 6803 respectively) and compared to that of the bootstrapping cross validation runs (i.e., 9.3 % and 18.8 % for PCC 11901 and PCC 6803 respectively). From this analysis, a 4.5 % prediction improvement in PCC 11901 and 3.1 % prediction deterioration in PCC 6803, respectively, were observed under uncertainty. The former percentage improvement was expected for the two models (i.e., PCC 11901 and PCC 6803) as mildly

perturbing responsive model parameters have been shown by Anye Cho *et al*., [27] to improve prediction accuracy. However, the unexpected prediction deterioration in PCC 6803 can be attributed to its noisy experimental data sets. Hence, the small 3.1 % prediction deterioration is expected to be reversed if presented with a less noisy experimental data sets since the simulation performance will be relatively high.

3.2.3 Overall comparison of the two cyanobacterial strains

As the prediction performance of the dynamic models for both the seen and the cross validated experimental datasets were within the wide operating range from 300 to 900 μmol photons m^{-2} s^{-1} , its full potential was then explored to address pertinent questions about the bioprocess dynamics, in particular: (i) which of the two cyanobacterial strains is fastest growing across a range of light intensities, (ii) what are their respective optimal light intensities, and (iii) does light intensity impact their upscaling potentials?

From the growth characteristics of the two strains outlined in Table 3, it was observed that the maximum specific growth rate of PCC 91101 was over two fold higher than that of PCC 6803. Whilst this increase was consistent with the experimental data sets, the order of magnitude was however about four-fold higher when comparing the final biomass concentration and optical densities as illustrated in Table 4. These disparities indicate that the results outlined in Table 4 are insufficient for characterising the strain specific growth properties as the dynamic model and estimated parameters can predict these results, but the reverse is not possible. Nonetheless, the faster growth of PCC 11901 agrees with previous studies [8,10], which demonstrated that it was superior to other 'fast' growing cyanobacterial strains like UTEX 2973 and PCC 7002. The light saturation coefficient of PCC 6803 was about two-fold lower than that of PCC 11901, indicating superior light affinity and utilisation efficiency. This implies PCC 6803 should be the faster growing strain which contradicts previous literature findings [8,10]. Explaining this

inconsistency is far beyond the capabilities of the linearised curve fitting literature methods for estimating and comparing maximum specific growth rate. This was addressed with the dynamic mechanistic modelling approach by analysing the maximum specific growth and decay rates in Table 3. Those of PCC 6803 were seen to be of similar order of magnitudes while the decay rate of PCC 11901 was about 67-fold lower than its maximum specific growth rate. This implies that for the portion of absorbed and utilised light intensities within the 300 to 900 µmol photons m^{-2} s^{-1} range, PCC 11901 was experiencing unbalanced growth dominating Eqs. (3) and (4), whereas that of PCC 6803 was balanced. Hence, the higher light affinity and utilisation efficiency of PCC 6803 compared to PCC 11901 was not directed towards growth promoting activities and was herein interpreted to be either for (i) cell maintenance, and/or (ii) fluorescence heat generation. Cell maintenance encompasses non-growth related metabolic activities performed by the cells to stay alive which usually consume energy in the form of adenosine triphosphate (ATP). Since ATP and nicotinamide adenine dinucleotide phosphate (NADPH) are the products of light dependent reactions [41], it was reasonable to assume that ATP and NADPH generation in PCC 6803 was mostly directed towards cell maintenance and not for carbon fixation via Calvin-Benson-Basshan cycle. This assumption was reasonably valid as the final biomass concentration ultimately derived from carbon fixation did not change within the investigated 300 to 900 µmol photons m^{-2} s^{-1} range. This also suggests that extra absorbed light above 300 µmol photons m^{-2} s^{-1} was mostly wasted as heat and not utilised for growth of PCC 6803 since Eqs. (3) and (4) were balanced.

The remaining two questions were only valid for PCC 11901 since the 300 to 900 µmol photons m^{-2} s^{-1} range were observed to be above the light intensity saturation threshold for PCC 6803, suggesting growth is light independent. As per the optimal light intensity of PCC 11901, the model derivative with respective to the light intensity was taken and equated to zero (i.e., $\frac{d\mu(I)}{dI} = 0$), thereby resulting in optimal light intensities, $I_{opt} = \sqrt{k_s \cdot k_I}$ of 727.0 µmol photons

m^{-2} s^{-1} and 742.9 µmol photons m^{-2} s^{-1} for the respective biomass and optical density models, respectively, and averaging 735.0 µmol photons m^{-2} s^{-1} to encompass both aspects. The similar I_{opt} values between both models (i.e., biomass and OD_{750nm}) suggest that they can be used interchangeably for (i) optimal design of experiments, and (ii) online bioprocess control since OD_{750nm} measurements with a UV/VIS spectrophotometer are more easily obtained over quantifying biomass. Second, these predicted optimal values are within the range of several other cyanobacterial species [8,10,42], supporting their validity. Although I_{opt} was slightly lower than the optimal 750.0 µmol photons m^{-2} s^{-1} reported highest biomass and OD_{750nm} from experimental data (i.e., I_{0_opt}), the 15 µmol photons m^{-2} s^{-1} difference was negligibly small (circa 2 %) and indicates the accurate dynamic estimation of k_s and k_I under the PBR light path length with 20-step trapezoidal approximations.

Next, we considered whether the upscaling potential of PCC 11901 will be severely impacted by light intensity. The light absorption coefficient was identified as the main parameter to be compared against values from photobioreactors of different scales and configurations. This was motivated by the intrinsic nature of the light absorption coefficient to cyanobacteria and the light attenuation challenges being the primary limitation for upscaling photobiological processes, as was investigated by Anye Cho *et al.*, [19]. Therefore, a high light absorption coefficient would indicate rapid diminishing local light transmissions within the PBR as its diameter was increased for upscaling, and vice-versa. The PCC 11901 light absorption coefficient compared well to that observed in previous studies [22,23] (i.e., $67 \leq \tau \leq 225$ mm^2 g^{-1}) outlined in Table 3. This suggests that upscaling of PCC 11901 cultivation will not be severely impacted by light intensity since previous studies used PBRs ranging from 0.5 L cylindrical PBRs [43,44], 1.0 L flat-plate [21,23] and tubular [45] PBRs, to as large as 120.0 L flat-plate PBRs [46,47].

4. Conclusions

In this investigation, experimental observation of biomass concentrations and optical densities, and statistical analysis with student's *t*-test were jointly exploited to support the incorporation of various photomechanisms within the dynamic mechanistic models of two cyanobacterial strains: PCC 11901 and PCC 6803. Whilst such models for OD_{750nm} were previously unavailable, the similarities of their growth profile to biomass models justified the existence of similar model structures and was herein implemented for the first time. Even so, the model for PCC 11901 embedded the complicated influences of incident light intensity, light attenuation and photomechanisms, whereas the one for PCC 6803 was only limited by the incident light intensity and photosaturation mechanisms. To simultaneously estimate the model parameter values and their associated confidence intervals, bootstrapping techniques with 3-fold cross validations was implemented. Thereafter, the models' predictions under uncertainties were thoroughly validated against unseen experimental data sets with small simulation errors averaging less than 19 %. Of the two species, PCC 11901 showed superior prediction fidelities and faster growth. Whilst fluorometry measurements are recommended in future for confirming the light-stressed photosynthetic activities of PCC 6803 within the 300 to 900 μmol photons m^{-2} s^{-1} range, further model-based analysis was carried out on the PCC 11901 model parameters. As a result, 735.0 μmol photons m^{-2} s^{-1} was identified as the optimal cultivation light intensity, and without severe light limitations during bioprocess upscaling. Therefore, these presented findings will benefit future biotechnological upscaling, online bioprocess control and exploitation of these strains.

Acknowledgement

B.A.C. acknowledges funding from the Commonwealth Scholarship Commission, United Kingdom. J.A.M.C. acknowledges funding support from a FEBS short term fellowship and University of Cordoba fellowship. L.A.M. acknowledge funding support from the BBSRC Norwich Research Park Doctoral Training Partnership program (grant number BB/S507404/1).

References

[1] Lindberg P, Park S, Melis A. Engineering a platform for photosynthetic isoprene production in cyanobacteria, using Synechocystis as the model organism. Metab Eng 2010;12:70–9. https://doi.org/10.1016/j.ymben.2009.10.001.

[2] Niederholtmeyer H, Wolfstädter BT, Savage DF, Silver PA, Way JC. Engineering cyanobacteria to synthesize and export hydrophilic products. Appl Environ Microbiol 2010;76:3462–6. https://doi.org/10.1128/AEM.00202-10.

[3] Balskus EP, Walsh CT. The Genetic and Molecular Basis for Sunscreen Biosynthesis in Cyanobacteria. Science (1979) 2010;329:1653–6. https://doi.org/10.1126/science.1193637.

[4] Brilisauer K, Rapp J, Rath P, Schöllhorn A, Bleul L, Weiß E, et al. Cyanobacterial antimetabolite 7-deoxy-sedoheptulose blocks the shikimate pathway to inhibit the growth of prototrophic organisms. Nat Commun 2019;10. https://doi.org/10.1038/s41467-019-08476-8.

[5] Pilon L, Berberoğlu H, Kandilian R. Radiation transfer in photobiological carbon dioxide fixation and fuel production by microalgae. J Quant Spectrosc Radiat Transf 2011;112:2639–60. https://doi.org/10.1016/j.jqsrt.2011.07.004.

[6] Collotta M, Champagne P, Mabee W, Tomasoni G. Wastewater and waste CO2 for sustainable biofuels from microalgae. Algal Res 2018;29:12–21. https://doi.org/10.1016/j.algal.2017.11.013.

[7] Roh H, Lee JS, Choi H il, Sung YJ, Choi SY, Woo HM, et al. Improved CO2-derived polyhydroxybutyrate (PHB) production by engineering fast-growing cyanobacterium

Synechococcus elongatus UTEX 2973 for potential utilization of flue gas. Bioresour Technol 2021;327:124789. https://doi.org/10.1016/j.biortech.2021.124789.

[8] Mills LA, Moreno-Cabezuelo JÁ, Włodarczyk A, Victoria AJ, Mejías R, Nenninger A, et al. Development of a Biotechnology Platform for the Fast-Growing Cyanobacterium Synechococcus sp. PCC 11901. Biomolecules 2022;12:872. https://doi.org/10.3390/biom12070872.

[9] Yu J, Liberton M, Cliften PF, Head RD, Jacobs JM, Smith RD, et al. Synechococcus elongatus UTEX 2973, a fast growing cyanobacterial chassis for biosynthesis using light and CO_2 . Sci Rep 2015;5:8132. https://doi.org/10.1038/srep08132.

[10] Włodarczyk A, Selão TT, Norling B, Nixon PJ. Newly discovered Synechococcus sp. PCC 11901 is a robust cyanobacterial strain for high biomass production. Commun Biol 2020;3. https://doi.org/10.1038/s42003-020-0910-8.

[11] Clark RL, McGinley LL, Purdy HM, Korosh TC, Reed JL, Root TW, et al. Light-optimized growth of cyanobacterial cultures: Growth phases and productivity of biomass and secreted molecules in light-limited batch growth. Metab Eng 2018;47:230–42. https://doi.org/10.1016/j.ymben.2018.03.017.

[12] Jaiswal D, Sengupta A, Sohoni S, Sengupta S, Phadnavis AG, Pakrasi HB, et al. Genome Features and Biochemical Characteristics of a Robust, Fast Growing and Naturally Transformable Cyanobacterium Synechococcus elongatus PCC 11801 Isolated from India. Sci Rep 2018;8:1–13. https://doi.org/10.1038/s41598-018-34872-z.

[13] Lea-Smith DJ, Vasudevan R, Howe CJ. Generation of marked and markerless mutants in model cyanobacterial species. Journal of Visualized Experiments 2016;2016:1–12. https://doi.org/10.3791/54001.

[14] Snoep JL, Mrwebi M, Schuurmans JM, Rohwer JM, Teixeira de Mattor MJT. Control of specific growth rate in Saccharomyces cerevisiae. Microbiology (N Y) 2009;155:1699–707. https://doi.org/10.1099/mic.0.023119-0.

[15] Zhang D, Dechatiwongse P, Del-Rio-Chanona EA, Hellgardt K, Maitland GC, Vassiliadis VS. Analysis of the cyanobacterial hydrogen photoproduction process via model identification and process simulation. Chem Eng Sci 2015;128:130–46. https://doi.org/10.1016/j.ces.2015.01.059.

[16] del Rio-Chanona EA, Dechatiwongse P, Zhang D, Maitland GC, Hellgardt K, Arellano-Garcia H, et al. Optimal Operation Strategy for Biohydrogen Production. Ind Eng Chem Res 2015;54:6334–43. https://doi.org/10.1021/acs.iecr.5b00612.

[17] Dechatiwongse P, Srisamai S, Maitland G, Hellgardt K. Effects of light and temperature on the photoautotrophic growth and photoinhibition of nitrogen-fixing cyanobacterium Cyanothece sp. ATCC 51142. Algal Res 2014;5:103–11. https://doi.org/10.1016/j.algal.2014.06.004.

[18] Lea-Smith DJ, Bombelli P, Dennis JS, Scott SA, Smith AG, Howe CJ. Phycobilisome-deficient strains of synechocystis sp. PCC 6803 have reduced size and require carbon-limiting conditions to exhibit enhanced productivity. Plant Physiol 2014;165:705–14. https://doi.org/10.1104/pp.114.237206.

[19] Anye Cho B, Carvalho Servia MÁ, del Río Chanona EA, Smith R, Zhang D. Synergising biomass growth kinetics and transport mechanisms to simulate light/dark cycle effects on photo- production systems. Biotechnol Bioeng 2021;118:1932–42. https://doi.org/10.1002/bit.27707.

[20] Cordara A, Re A, Pagliano C, van Alphen P, Pirone R, Saracco G, et al. Analysis of the light intensity dependence of the growth of Synechocystis and of the light

distribution in a photobioreactor energized by 635 nm light. PeerJ 2018;2018:1–28. https://doi.org/10.7717/peerj.5256.

[21] Zhang D, Dechatiwongse P, Hellgardt K. Modelling light transmission , cyanobacterial growth kinetics and fl uid dynamics in a laboratory scale multiphase photo-bioreactor for biological hydrogen production. Algal Res 2015;8:99–107. https://doi.org/10.1016/j.algal.2015.01.006.

[22] Zhang D, Dechatiwongse P, del Rio-Chanona EA, Maitland GC, Hellgardt K, Vassiliadis VS. Dynamic modelling of high biomass density cultivation and biohydrogen production in different scales of flat plate photobioreactors. Biotechnol Bioeng 2015;112:2429–38. https://doi.org/10.1002/bit.25661.

[23] Zhang D, Dechatiwongse P, del Rio-Chanona EA, Maitland GC, Hellgardt K, Vassiliadis VS. Modelling of light and temperature influences on cyanobacterial growth and biohydrogen production. Algal Res 2015;9:263–74. https://doi.org/10.1016/j.algal.2015.03.015.

[24] Williams JGK. Construction of Specific Mutations in Photosystem II Photosynthetic Reaction Center by Genetic Engineering Methods in Synechocystis 6803. Methods Enzymol 1988;167:766–78. https://doi.org/10.1016/0076-6879(88)67088-1.

[25] Cornet JF, Dussap CG, Gros JB, Binois C, Lasseur C. A simplified monodimensional approach for modeling coupling between radiant light transfer and growth kinetics in photobioreactors. Chem Eng Sci 1995;50:1489–500. https://doi.org/10.1016/0009-2509(95)00022-W.

[26] Pottier L, Pruvost J, Deremetz J, Cornet J-F, Legrand J, Dussap CG. A fully predictive model for one-dimensional light attenuation byChlamydomonas reinhardtii in a torus

photobioreactor. Biotechnol Bioeng 2005;91:569–82. https://doi.org/10.1002/bit.20475.

[27] Anye Cho B, Ross BS, du Toit JP, Pott RWMC, del Río Chanona EA, Zhang D. Dynamic modelling of Rhodopseudomonas palustris biohydrogen production: Perturbation analysis and photobioreactor upscaling. Int J Hydrogen Energy 2021;46:36696–708. https://doi.org/10.1016/j.ijhydene.2021.08.162.

[28] Palamae S, Choorit W, Dechatiwongse P, Zhang D, Antonio del Rio-Chanona E, Chisti Y. Production of renewable biohydrogen by Rhodobacter sphaeroides S10: A comparison of photobioreactors. J Clean Prod 2018;181:318–28. https://doi.org/10.1016/j.jclepro.2018.01.238.

[29] Wächter A, Biegler LT. On the implementation of an interior-point filter line-search algorithm for large-scale nonlinear programming. Math Program 2006;106:25–57. https://doi.org/10.1007/s10107-004-0559-y.

[30] Nicholson B, Siirola JD, Watson JP, Zavala VM, Biegler LT. Pyomo.Dae: a Modeling and Automatic Discretization Framework for Optimization With Differential and Algebraic Equations. Math Program Comput 2018;10:187–223. https://doi.org/10.1007/s12532-017-0127-0.

[31] Hart WE, Laird C, Watson J-P, Woodruff DL. Pyomo – Optimization Modeling in Python. vol. 67. Boston, MA: Springer US; 2012. https://doi.org/10.1007/978-1-4614-3226-5.

[32] Mowbray M, Savage T, Wu C, Song Z, Cho BA, del Rio-Chanona EA, et al. Machine learning for biochemical engineering: A review. Biochem Eng J 2021;172:108054. https://doi.org/10.1016/j.bej.2021.108054.

[33] Rogers AW, Vega-Ramon F, Yan J, del Río-Chanona EA, Jing K, Zhang D. A transfer learning approach for predictive modeling of bioprocesses using small data. Biotechnol Bioeng 2022;119:411–22. https://doi.org/10.1002/bit.27980.

[34] Pinto J, de Azevedo CR, Oliveira R, von Stosch M. A bootstrap-aggregated hybrid semi-parametric modeling framework for bioprocess development. Bioprocess Biosyst Eng 2019;42:1853–65. https://doi.org/10.1007/s00449-019-02181-y.

[35] Tyystja¨rvi ET, Hakala M, Sarvikas P. Mathematical modelling of the light response curve of photoinhibition of Photosystem II. n.d.

[36] Baker NR. Chlorophyll fluorescence: A probe of photosynthesis in vivo. Annu Rev Plant Biol 2008;59:89–113. https://doi.org/10.1146/annurev.arplant.59.032607.092759.

[37] Gerken-Starepravo L, Zhu X, Cho BA, Vega-Ramon F, Pennington O, Antonio del Río-Chanona E, et al. An MIQP framework for metabolic pathways optimisation and dynamic flux analysis. Digital Chemical Engineering 2022;2:100011. https://doi.org/10.1016/j.dche.2022.100011.

[38] Pinto J, de Azevedo CR, Oliveira R, von Stosch M. A bootstrap-aggregated hybrid semi-parametric modeling framework for bioprocess development. Bioprocess Biosyst Eng 2019;42:1853–65. https://doi.org/10.1007/s00449-019-02181-y.

[39] Cabello J, Morales M, Revah S. Dynamic photosynthetic response of the microalga Scenedesmus obtusiusculus to light intensity perturbations. Chemical Engineering Journal 2014;252:104–11. https://doi.org/10.1016/j.cej.2014.04.073.

[40] Sadino-Riquelme MC, Rivas J, Jeison D, Hayes RE, Donoso-Bravo A. Making sense of parameter estimation and model simulation in bioprocesses. Biotechnol Bioeng 2020;117:1357–66. https://doi.org/10.1002/bit.27294.

[41] Carvalho AP, Silva SO, Baptista JM, Malcata FX. Light requirements in microalgal photobioreactors: An overview of biophotonic aspects. Appl Microbiol Biotechnol 2011;89:1275–88. https://doi.org/10.1007/s00253-010-3047-8.

[42] Salleh SF, Kamaruddin A, Uzir MH, Mohamed AR, Shamsuddin AH. Modeling the light attenuation phenomenon during photoautotrophic growth of A. variabilis ATCC 29413 in a batch photobioreactor. Journal of Chemical Technology and Biotechnology 2017;92:358–66. https://doi.org/10.1002/jctb.5013.

[43] Rivera C, Niño L, Gelves G. Modeling of phycocyanin production from Spirulina platensis using different light-emitting diodes. S Afr J Chem Eng 2021;37:167–78. https://doi.org/10.1016/j.sajce.2021.05.005.

[44] del Rio-Chanona EA, Liu J, Wagner JL, Zhang D, Meng Y, Xue S, et al. Dynamic modeling of green algae cultivation in a photobioreactor for sustainable biodiesel production. Biotechnol Bioeng 2018;115:359–70. https://doi.org/10.1002/bit.26483.

[45] Rio-chanona EA, Ahmed N rashid, Zhang D, Lu Y, Jing K. Kinetic Modeling and Process Analysis for Desmodesmus sp. Lutein Photo-Production. AICHE Journal 2017;63:2546–54. https://doi.org/10.1002/aic.

[46] del Rio-Chanona EA, Wagner JL, Ali H, Fiorelli F, Zhang D, Hellgardt K. Deep learning-based surrogate modeling and optimization for microalgal biofuel production and photobioreactor design. AIChE Journal 2019;65:915–23. https://doi.org/https://doi.org/10.1002/aic.16473.

[47] Ali H, Solsvik J, Wagner JL, Zhang D, Hellgardt K, Park CW. CFD and kinetic- based modeling to optimize the sparger design of a large- scale photobioreactor for scaling up of biofuel production. Biotechnol Bioeng 2019;116:2200–11. https://doi.org/10.1002/bit.27010.